https://doi.org/10.5194/egusphere-2025-485
Preprint. Discussion started: 16 May 2025

Quantifying Forest Canopy Shading and Turbulence Effects on Boundary Layer Ozone over the United States

Chi-Tsan Wang[1], Patrick C. Campbell[1,2,3,*], Paul Makar[4] , Siqi Ma[1] , Irena Ivanova[1,2,3], Bok H. Baek[1], Wei-Ting Hung[1,2,3], Zachary Moon[5], Youhua Tang[1,2,3], Barry Baker[3], Rick Saylor[3], and Daniel Tong[1]

[1] Center for Satellite and Earth Science Research (CSER), George Mason University, Fairfax, VA, USA

[2] Cooperative Institute for Satellite Earth System Studies (CISESS), George Mason University, Fairfax, VA, USA

[3]NOAA Air Resources Laboratory, College Park, MD, USA

[4] Environment and Climate Change Canada (ECCC), Toronto, ON, Canada.

[5] Earth Resources Technology, Inc., Laurel, MD, USA

[*]Corresponding authors: Patrick C. Campbell (Email: patrick.c.campbell@noaa.gov; Telephone:307-760-5178)

Abstract

The presence of dense forest canopies significantly alters the near-field dynamical, physical, and chemical environment, with implications for atmospheric composition and air quality variables such as boundary layer ozone (O_3). Observations show profound vertical gradients in O_3 concentration beneath forest canopies; however, most chemical transport models (CTMs) used in the operational and research community, such as the Community Multiscale Air Quality (CMAQ) model, cannot account for such effects due to inadequate canopy representation and lack of sub-canopy processes. To address this knowledge gap, we implemented detailed forest canopy processes—including in-canopy photolysis attenuation and turbulence—into the CMAQv5.3.1 model, driven by the Global Forecast System and enhanced with high-resolution vegetation datasets. Simulations were conducted for August 2019 over the contiguous U.S. The canopy-aware model shows substantial improvement, with mean O_3 bias reduced from +0.70 ppb (Base) to −0.10 ppb (Canopy), and fractional bias from +9.71% to +6.37%. Monthly mean O_3 in the lowest model layer (~0–40 m) decreased by up to 9 ppb in dense forests, especially in the East. Process analysis reveals a 75.2% drop in first-layer O_3, with daily surface production declining from 673 to 167

https://doi.org/10.5194/egusphere-2025-485
Preprint. Discussion started: 16 May 2025

ppb d^{-1}, driven by suppressed photolysis and vertical mixing. This enhances NO_x titration and reduces O_3 formation under darker, stable conditions. The results highlight the critical role of canopy processes in atmospheric chemistry and demonstrate the importance of incorporating realistic vegetation-atmosphere interactions in CTMs to improve air quality forecasts and health-relevant exposure assessments.

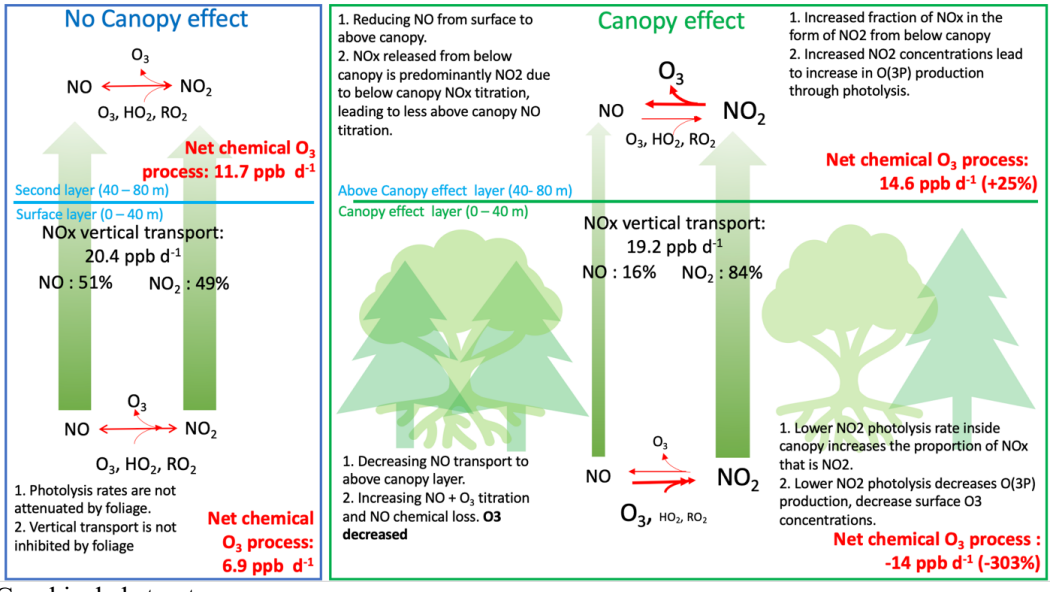

Graphical abstract:

1. Introduction

The Earth's vegetative canopies have ubiquitous effects on the physical, dynamical, and chemical environments, that impact the fluxes of momentum, heat, water, nutrients, and gases to the atmosphere above the canopy (Bonan et al., 2021; Bonan et al., 2018; Bonan et al., 2014). Some primary processes that alter the chemistry of the Earth's atmosphere due to the within canopy environment include radiative transport and photolysis(Monsi, 1953; Nilson, 1971; Makar et al., 2017; Moon et al., 2020; Norman, 1979), turbulent transport and diffusion (Raupach, 1989; Harman and Finnigan, 2007, 2008; Ashworth et al., 2015; Makar et al., 2017; Bonan et al., 2018), and hydrocarbon and other trace gas emissions (Guenther et al., 2012) and deposition to the leaves and foliage (Vermeuel et al., 2023). Understanding the importance of near-surface and canopy environments has led to decades-long measurements of heat, momentum, and trace gases and aerosols fluxes across different land surface types, vegetation properties, and forest/tree canopy characteristics (Baldocchi and Harley, 1995; Meyers et al., 1998; Hicks et al., 2016; Saylor et al., 2019; Hicks and Baldocchi, 2020). More recent field campaigns such as the Flux Closure Study 2021 (FLUCS 2021) have studied the complex forest canopy chemistry and fluxes (e.g., reactive

https://doi.org/10.5194/egusphere-2025-485
Preprint. Discussion started: 16 May 2025

carbon fluxes) to attempt at closing budgets critical to atmospheric composition modeling across scales (Vermeuel et al., 2023).

Widely used chemical transport models (CTMs) in the community, such as the Community Multiscale Air Quality (CMAQ) model (Byun, 1999; Byun and Schere, 2006), have well represented processes that govern the Earth's atmospheric composition and air quality, including anthropogenic/natural source emissions, gas and aqueous chemistry, aerosol formation and physics, resolved horizontal/vertical transport, and dry/wet deposition (Appel et al., 2021); however, those CTMs often largely rely on the "big-leaf" approach that has minimal representation of sub-canopy structure and explicit processes (Bash et al., 2013; Pleim and Ran, 2011; Pleim et al., 2019; Pleim et al., 2022). The big-leaf approach is readily used in land, weather, climate, and CTMs, and represents the plant canopies as a homogeneous single layer without real vertical structure (Bonan et al., 2021). This approach might be considered a reasonable simplification when atmospheric models routinely used horizontal resolutions (> 20 km) where a largely heterogeneous landscape within each grid cell could be represented only approximately anyway. Now, as horizontal resolutions of weather, climate and air quality models are becoming smaller and smaller, the adequacy of the big-leaf approach is being called into question. In addition, the big leaf models and the chemical transport models in which they reside did not take into account the potential impact of changes in the vertical coordinate between the below-canopy and above-canopy environment (e.g. changes in light and temperature levels) on atmospheric chemistry, and of the vertical transport of pollutants from below- to above-canopy.

As an alternative to the big-leaf, single-layer canopy representations in CTMs, multilayer canopy models can resolve vertically varying profiles and microclimates in canopies (Baldocchi and Harley, 1995; Ogée et al., 2003; Chang et al., 2018; Bonan et al., 2021). The vertical distribution of leaf area has substantial impacts on the microclimate, leaf morphology, and leaf physiology in forest canopies, which in turn drives the dynamic/kinematic (e.g., wind speed and turbulent kinetic energy profiles), thermodynamic and radiative effects (e.g., daytime/nighttime air temperatures and light levels within and below the canopy) (see Bonan et al., 2021 and references found within). These in turn may drive and chemical responses associated with the below-canopy environment to these changes (e.g., trace gas/scalar transport) characteristics of the sub-canopy layer. The use of a single-layer, "big-leaf" approach neglects such in-canopy profiles and their consequences, under the driving desire to adequately reproduce the behavior of multi-layer canopies to derive bulk quantities such as evapotranspiration from the canopy, and gross primary production. While the big-leaf simplification has over time proven useful in the sense that it is computationally efficient and can provide reasonably accurate fluxes, it can only be assumed to be "correct" under certain applications, namely large-scale influences of vegetation on large-scale climate (i.e., it is a "useful" approach). However, to best understand how large-scale climate effects manifest in the local, vertical, microclimate associated with vegetation, requires the use of

https://doi.org/10.5194/egusphere-2025-485
Preprint. Discussion started: 16 May 2025

in-canopy parameterizations or more comprehensive multi-layer canopy (MLC) models. Furthermore, MLCs are explicitly needed to simulate chemistry and scalar transport in forest canopies (Boy et al., 2011; Wolfe and Thornton, 2011; Bryan et al., 2012; Saylor, 2013; Bonan et al., 2014; Ashworth et al., 2015). Overall, explicit in-canopy modeling can also better handle the natural complexity of trace gas and aerosol fluxes between the surface, vegetation, and atmosphere that are known to be important to Earth System, biogeochemical budgets (Braghiere et al., 2019).

MLC models have been incorporated in research versions of regional (e.g., Weather Research and Forecasting Model; (Xu et al., 2017)) and global (Community Land Model; Bonan et al., 2014, 2018) weather and climate models, and these previous studies have generally shown that the more detailed canopy representations can increase model accuracy in evapotranspiration. The understanding of the impact of the multilayer canopy on turbulence, and scalar transport has been long known (Raupach, 1989), and has been applied to one-dimensional canopy models that show good agreement with observations (Makar et al., 1999; Stroud et al., 2005; Saylor, 2013; Gordon et al., 2014; Ashworth et al., 2015). Only more recently have the effects of multilayer canopy models been scaled up to large eddy simulations with chemistry (Clifton et al., 2022; Fuentes et al., 2022) and to regional scale air quality forecast (AQF) models with more complex chemistry (Makar et al., 2017). Here, one of our main aims was to evaluate the effects of these processes in a regional scale CTM, CMAQ, in the community. A major limitation is that MLC models are more computationally costly and have proven problematic for widespread use and understanding in complex CTMs, necessitating the need for parameterized or simplified forms of these models that may reside within a more complex CTM, and capture the main features of the MLC models.

The CTMs used in the community and in operational forecasting centers continue to generate systematic ozone (O_3) overpredictions in the eastern U.S. during the photochemical summer O_3 season (e.g., July-August). Such biases have been linked to distinct vertical gradients of O_3 measured within dense forest canopies of the U.S. (Makar et al., 2017). Most CTMs and air quality forecasting models cannot capture such details, as they continue to rely on the previously discussed big-leaf model to represent canopy interactions with chemistry and scalar transport (Makar et al., 2017; Bonan et al., 2021). However, Makar et al. (2017) showed that inclusion of explicit sub-canopy effects of photolysis and the attenuation of light, in combination with the effects of sub-canopy vertical diffusivity in a regional-scale CTM, can improve predictions of near-surface O_3 concentrations in regions of contiguous canopies. It was further noted that simulated tropospheric O_3 in forest canopy regions is significantly reduced, through the combined effects of forest canopy shading (about ⅓ of the total reduction) and modified turbulence (the remaining ⅔), and that the inclusion of these in-canopy processes can largely correct this long-standing positive bias in forecasts of near-surface O_3 in the eastern U.S. across multiple air-quality models (Makar et al., 2017).

https://doi.org/10.5194/egusphere-2025-485
Preprint. Discussion started: 16 May 2025

The objectives of this work are to adapt the methodologies from Makar et al. (2017) and integrate them into relatively simple, but efficient parameterizations of in-canopy photolysis and turbulent diffusivity effects in the widely used CMAQ model. We then employ CMAQ process-analysis (PA) techniques, to better discern and quantify the in-canopy photolysis/chemistry and turbulence/transport effects on O_3 and other related chemical species and processes over the entire contiguous U.S. region (CONUS). Apart from Makar et al. (2017), most studies on in-canopy chemistry and turbulence/diffusivity effects have been applied at local/field to near-local scales, while regional scale CTMs can better represent the widespread effects of in-canopy chemistry, turbulent diffusivity, and vertical transport across CONUS, and show how in-canopy processes interact with other processes in the atmosphere (such as advective transport and feedbacks between the canopy effects and meteorology). We focus on primary effects of in-canopy chemistry and turbulence in CMAQ, and do not cover the secondary effects of in-canopy structure on emissions and dry deposition here. Section 2 describes the methods of the CMAQ model canopy parameterizations, CMAQ PA approaches, simulation design, observations, and evaluation protocol. Section 3 shows the results of the in-canopy parameterizations in CMAQ on O_3 and NO_x, and a detailed evaluation and analysis of the impacts. Section 4 provides the study's main conclusions, a discussion on the limitations of the parameterizations, and paths forward to further improve integration of more comprehensive in-canopy processes for atmospheric composition models across scales.

https://doi.org/10.5194/egusphere-2025-485
Preprint. Discussion started: 16 May 2025

2. Methods

2.1 Gridded canopy datasets and contiguous canopy thresholds for CMAQ

A suite of gridded vegetative canopy-related parameters is needed for the new in-canopy parameterizations in CMAQ, as well as to define what model grid cells are representative of a contiguous canopy. These parameters include gridded 2-D fields such as the leaf area index (LAI), forest canopy height (FCH), forest fraction (FRT), and forest clumping index (CLU) based on Makar et al. (2017)(Figure 1). These four canopy parameters are derived from a suite of ground-based datasets and space-borne observations including the MODerate Resolution Imaging Spectrometers (MODIS) on the NASA Terra and Aqua satellites. An additional dataset, population density (POPU), is used to identify and filter out city core areas that do not have contiguous vegetated canopies. To further approximate the vertical canopy structure spatially across the domain, we define four additional variables using the total LAI and cumulative LAI fractions (CLAI_FRAC) at four FCH-relative heights (0.75*FCH, 0.50*FCH, 0.35*FCH, and 0.20*FCH) within the canopy (Figure 1). These heights were chosen to resolve the typical turbulence structure within forest canopies (Makar et al., 2017, Raupach, 1989). The CLAI_FRAC is based on typical leaf vertical distributions from the literature for different forest types (deciduous, coniferous, and mixed forests) assigned to the 230 Biogenic Emissions Landuse Database (BELD), version 3 (Pierce et al., 1998). These BELD data were weighted by the associated MODIS-based land use fractions in the model grid cell, and similar methods were used for CLU. More details on retrieval and processing of the gridded canopy variables may be found in Makar et al. (2017).

The first step in parameterization of the vegetative in-canopy effects is to determine whether a CMAQ model grid cell is defined as having a contiguous canopy with sufficient foliage to warrant defining a canopy column and correction. Based on similar theory from Makar et al. (2017), we apply the following canopy thresholds to define if a grid cell has a contiguous forest canopy:

1. The LAI is relatively small (i.e., less likely to have canopy shading or turbulence changes). *LAI > 0.1.*
2. The FCH is reasonably lower (< 25% of the lowest model layer depth, ~ 40 meters; see Section 2.3 and Table 1) in vertical extent that it will be a small fraction of the resolved meteorological model's lowest layer depth. *FCH > 10 m.*
3. The POPU is high enough to indicate the grid cell represents a large city. *POPU < 10,000 people per10 km^2 = 1,000 people/km^2.*
4. The FRT suggests that a contiguous forest canopy is unlikely (e.g., only half of the land use in the grid cell is forested). *FRT > 0.5.*
5. Too much of the incident light (i.e., the solar zenith angle; θ) makes it to the ground and the canopy is relatively short (i.e., minimal shading and turbulence changes would be expected). In this case, the threshold is defined as if more than 55% of the incident light makes it to the

https://doi.org/10.5194/egusphere-2025-485
Preprint. Discussion started: 16 May 2025

ground and the canopy is less than 18 m in height. *EXP(-0.5*LAI*CLU) < 0.45 and FCH > 18 m*.

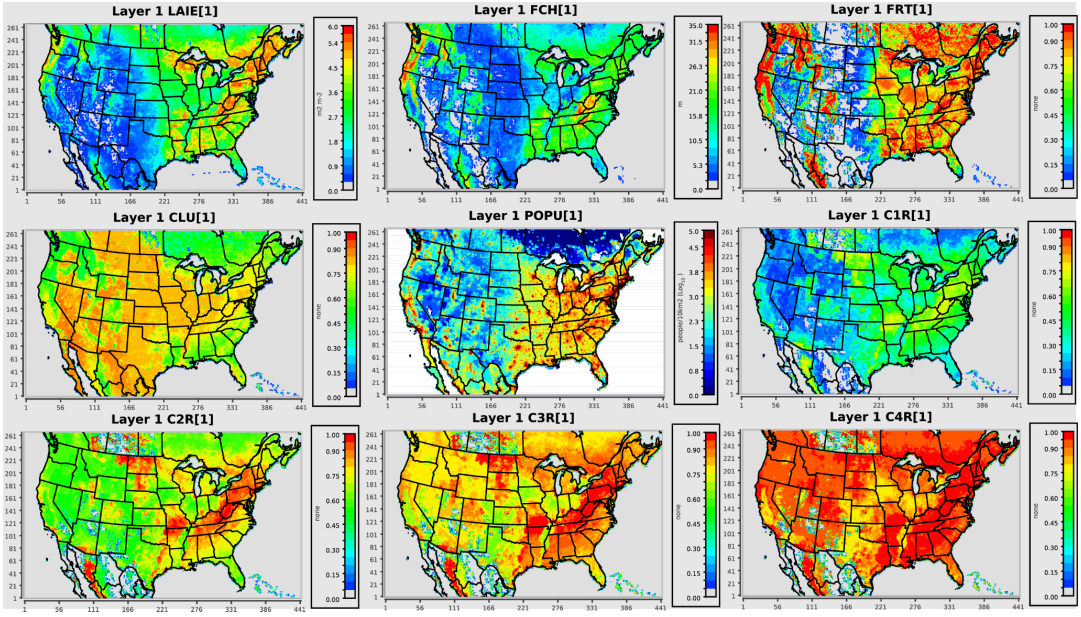

Figure 1. Spatial plots of average LAI, FCH, FRT, CLU, POPU, and CLAI_FRAC1-4 (referred to as C1R-C4R in headers) used for August 2019 CMAQ simulations in this work.

We note that our FCH contiguous canopy condition #2 above (FCH >10 m) updates that of Makar et al. (2017), which used a much lower FCH threshold (FCH > 0.5 m). We arrived at the FCH > 10 m threshold after numerous tests experimenting with 0.5 m, 3 m, and 10 m (along with all other canopy conditions applied), which resulted in a current best-case scenario regarding accurate regions of contiguous forests in the U.S. simultaneously occurring with regions of CMAQ model systematic ozone overpredictions (See Supporting Figure S1). One implication of this finding is that vegetative canopies must be sufficiently "deep" for their effects to have an impact on regional scale atmospheric chemistry.

2.2. Vegetative In-Canopy Parameterizations in CMAQ

Here we describe the vegetative in-canopy parameterizations associated with the attenuation of light (photolysis) and the effects of modified turbulence (eddy diffusivity) based on Makar et al. (2017), as they have been implemented into the CMAQ model. We note that one significant difference in the implementation as described below is that the CTM vertical structure has been retained in its original form, unlike Makar et al (2017) where additional vertical layers were added locally within canopy grid cells and model processes were split to operate on both the original CTM layer structure (in non-canopy grid cells) and an enhanced layer structure (in canopy

https://doi.org/10.5194/egusphere-2025-485
Preprint. Discussion started: 16 May 2025

grid cells), the latter including three additional layers. Here, the approach is to determine the impact of the canopy effects on the regional model layer structure, through calculation of CTM layer-thickness weighted photolysis attenuation and turbulent diffusivity reductions. While this approach does not explicitly resolve the canopy structure, it does provide estimates of its impact on the resolved vertical scale, requires less computational resources than the introduction of spatially varying local layers, and does not require the larger effort of recoding the CTM's core. The implementation of the full canopy layer structure within CMAQ is being implemented in ongoing work (Ivanova, 2024).

In-Canopy Photolysis: Using representative canopy conditions, the impact of attenuation of light due to a contiguous forest canopy can be parameterized in CMAQ for the j'th model layer in the following way:

$$P(\theta,z) = \frac{\int_{z_{j-\frac{1}{2}}}^{z_{j+\frac{1}{2}}} \exp\left(-\frac{G(\theta)CLU(\theta)LAI(z)}{\cos(\theta)}\right)dz}{z_{j+\frac{1}{2}} - z_{j-\frac{1}{2}}} \qquad \text{Eq. (1)}$$

Where *P(θ,z)* is the probability of beam penetration (i.e., fractional light penetration; Nilson, 1971; Monsi and Saeki, 1953), and depends on the LAI, leaf projection (G; for spherical assumption = 0.5), CLU, and solar zenith angle (θ). To capture the canopy vertical structure (i.e., leaf vertical distributions) in Eq. (1), we note that the LAI is dependent on height within the vegetation (*LAI(z)*), and that above the forest canopy height (z > FCH), the LAI is zero and the exponential term returns a value of unity (no light attenuation). To parameterize the integral effect of *P(θ,z)*, we multiply the total LAI in the grid cell by the set of four CLAI_FRAC datasets (i.e.,g C1R-C4R) between the FCH and the four heights within the canopy (see Section 2.1 and Figure 1), thus deriving the height-dependent photolysis attenuation factor. Linear interpolation between these attenuation values gives the attenuation profile below FCH. This vertically averaged probability of beam penetration is used as a correction factor on the j'th layer photolysis rates used in the CMAQ chemistry gas solver, which in turn affects the subsequent predictions of O_3, trace gas, and particulate matter concentrations.

In-Canopy Turbulence: In CMAQ, the near-surface scalar transport in the vertical is based on Monin-Obukhov (M-O) similarity theory (Monin and Obukhov, 1954) and calculation of the eddy diffusivity coefficient (*K*). Without presence of in-canopy effects, this calculation is based on the resolved meteorology taken in the native first model layer (closest to the surface); however, the fluxes and profiles in and above rough plant canopies deviate from M-O similarity theory due to the presence of a roughness sublayer (Bonan et al., 2018), where scalar transport is dominated by localized turbulence rather than large-scale advection (i.e., M-O theory cannot be used). Following the Makar et al. (2017) application of the Raupach (1989) near-field theory for many one-dimensional canopy models in the literature, and similar to our approach for photolysis, we

https://doi.org/10.5194/egusphere-2025-485
Preprint. Discussion started: 16 May 2025

adapt a methodology of vertically weighting the resolved layer values by a reduction factor referenced to an above-canopy height z1, to parameterize in-canopy effects on turbulence/diffusivity in CMAQ, using the following two equations:

$$K_{can}(z) = \frac{\int_{z_{j-\frac{1}{2}}}^{z_{j+\frac{1}{2}}} \frac{K_{mod}(z_1)}{K_{est}(\frac{z_1}{FCH})} K_{est}(\frac{z}{FCH}) dz}{z_{j+\frac{1}{2}} - z_{j-\frac{1}{2}}} \quad \text{Eq. (2)}$$

$$(\frac{z}{FCH}) = \sigma_w^2(\frac{z}{FCH}) T_L \frac{z}{FCH} \quad \text{Eq. (3)}$$

where z is the height above the Earth's surface, z_1 is the height of the lowest model layer above the forest canopy, σ_w^2 the variance in Eulerian vertical velocity, T_L the Lagrangian turbulence timescale, and K_{mod} (z_1), σ_w^2 and T_L are dependent on the resolved friction velocity and atmospheric stability conditions from the driving meteorological model at the lowest model layer above the forest canopy (see Eqs. 4-9 in Makar et al., 2017), and that the effective in-canopy diffusivity, K_{can} (z), is normalized to allow a smooth transition between the K values for the resolved first model layer above the forest canopy and the reduced values within the forest canopy, K_{est} (z_1/FCH). Effectively, the original CTM turbulent diffusivity coefficient profile *Kmod(z)* is weighted by a reduction factor which takes into account the typical shape of the observed diffusivity profile between the region above the canopy and the surface. Here, this reduction has been vertically weighted to determine the net reduction in the CTM's vertical layer structure, in contrast to the approach in Makar et al. (2017) where additional vertical layers were explicitly added to the model vertical structure. The calculated values of K_{can} (z) are integrated downward through the sub-grid canopy in CMAQ at a vertical resolution of $\Delta z = 0.5$ m (same as for photolysis attenuation). The result is a reduction in the K values of the near-surface layers of the model (those containing forest canopies), and reducing the vertical transport of species within those model layers. This effectively introduces a separation in the above and below canopy environments, through reducing near-surface vertical transport in forest canopies. This can lead to higher concentrations of species emitted near the surface (e.g. NO) that in turn influence other species (for example O_3, through enhanced O_3 titration in the same region that the photolysis rate reduction is reducing NO_2 photolysis). The reductions in vertical diffusivity also reduce the vertical transport/mixing of near-surface O_3 with the adjacent model layers above the canopy. In synergy with the in-canopy photolysis attenuation effects, the modified vertical diffusivity can thus, in part, further reduce predicted near-surface O_3 concentrations, and typical CTM overpredictions in regions of contiguous canopies. We note that the in-canopy photolysis attenuation and turbulence/scalar transport parametrizations, as implemented here through vertical weighting of photolysis and turbulent diffusivity coefficient reductions for the CTM's vertical layers, add negligible computation time to the CMAQ routines, and are easier to implement in CTMs than the

https://doi.org/10.5194/egusphere-2025-485
Preprint. Discussion started: 16 May 2025

core model recoding required in the approach described in Makar et al. (2017). The relative impact of explicitly adding additional model layers to CMAQ is being examined in ongoing work. An additional important difference in the implementation here relative to Makar et al (2017) is that the modifications to the coefficients of forest canopy turbulence are applied the driving meteorological model itself (rather than the scaled coefficients only being applied to the vertical transport of chemical tracers, as in Makar et al, 2017I).

2.2 CMAQ Process Analysis

Process Analysis (PA) is a diagnostic tool ((Jeffries and Tonnesen, 1994; Henderson et al., 2010)) used to investigate and quantify complex processes leading to chemical concentration changes in the CMAQ model. The CMAQ model simulates the hourly air pollutant concentration, while PA provides the hourly process-based rates for selected air pollutants for each grid cell, including horizontal and vertical advection, diffusion, emission, dry/wet deposition, and chemical reaction rates (USEPA, 2022). Therefore, the PA diagnostics can be used to better quantify the effects of the forest canopy parameterizations and impacts on chemical concentrations in the CMAQ model. The PA results within chemical transport models (CTMs) include two key components: the integrated process rate (IPR), which accounts for hourly net chemical and physical processes, and the integrated reaction rate (IRR), which covers all chemical hourly reaction processing rates. The analysis tool, Python Environment for Reaction Mechanism/Mathematics (PERMM) (Henderson et al., 2009), is applied to study the IPR and IRR results. This study generated the hourly IPR data for O_3, nitrogen oxides ($NO+NO_2=NO_x$), volatile organic compounds (VOCs), and its composition for the simulated case studies (Section 2.3). The details of chemistry processing rates (initiation, propagation, and termination reactions) for all species in a reduced chemical mechanism (CB6r3) are used to quantify the O_3 and NO_x changes.

2.3 Simulation Design, Observations and Evaluation Protocol

The model configuration used to implement and investigate the in-canopy parameterizations (Section 2.2) is based on a variant of the offline CMAQ model, version 5.3.1 (Appel et al., 2021). The updated CMAQv5.3.1 forest canopy shading, and turbulent diffusivity model codes (based on Eqs. 1-3) are available at https://zenodo.org/records/14502375 and https://github.com/GMU-SESS-AQ/CMAQ/releases/tag/GMU_Canopy_CMAQv5.3.1_05Aug2024. The meteorological driver is based on NOAA's operational Finite Volume Cubed Sphere (FV3) Global Forecast System (GFS) version 16.2, which was processed for model-ready CMAQ input by the NOAA-EPA Atmospheric-Chemistry Coupler (NACC), version 2.1.2, which is available at https://github.com/noaa-oar-arl/NACC/releases/tag/v2.1.2 (Campbell, 2023; Campbell et al., 2022). NACC is used to bi-linearly interpolate the canopy-related variables from Makar et al.

https://doi.org/10.5194/egusphere-2025-485
Preprint. Discussion started: 16 May 2025

(2017) including LAI, FCH, FRT, CLU, POPU, and C1R-C4R into the CMAQ grid used here (Figure 1), which are needed for the updated forest canopy shading and turbulent diffusivity codes in CMAQ. These canopy variables are not available in the GFSv16.2 output files and thus are provided to NACC via external satellite and surface vegetation data sources (as discussed in Section 2.1), with conversion of these fields to the CMAQ grid being carried out through NACC). The overall meteorological and chemical model components, configurations, and other model inputs are shown in Table 1.

Table 1. The main meteorological (GFS) and chemical (CMAQ) model components and configurations used in this study. The abbreviation N/A stands for not applicable in this table.

Model attributes	**Configuration**	**Reference or Data Source**
Domain	Contiguous U.S. Centered on 40° N 97° W	N/A
Horizontal resolution	12 km	N/A
Vertical resolution	35 levels from near the surface up to the top of stratosphere, ~ 40m thick 1st and 2nd model layer	N/A
Meteorological ICs and BCs	FV3/GFSv16.2	https://nws.weather.gov/ (last access: 25 November 2023). Processed using NACC (Campbell et al., 2022; Campbell, 2023)
Chemical ICs and BCs	GEOS-Chem 2006	https://geoschem.github.io/
Microphysics	GFDL six-category cloud microphysics scheme	(Lin et al., 1983; Lord et al., 1984; Krueger et al., 1995; Chen and Lin, 2011, 2013)
PBL physics scheme	sa-TKE-EDMF	(Han and Bretherton, 2019)
Shallow and deep cumulus parameterization	SAS scheme	(Han and Pan, 2011; Han et al., 2017)
Shortwave and longwave radiation	RRTMg	(Mlawer et al., 1997; Clough et al., 2005; Iacono et al., 2008)
Land surface model	Noah land surface model	(Chen and Dudhia, 2001; Ek et al., 2003; Tewari, 2004)
Surface layer	Monin-Obukhov	(Monin and Obukhov, 1954; Grell, 1994; Jiménez et al., 2012)
Gas-phase chemistry	CB6r3	(Yarwood et al., 2010)
Aqueous-phase chemistry	CMAQ AQChem updates	(Martin and Good, 1991; Alexander et al., 2009; Sarwar, 2011)
Aerosol module	AERO7	(Appel et al., 2021)

https://doi.org/10.5194/egusphere-2025-485
Preprint. Discussion started: 16 May 2025

Anthropogenic emissions	U.S. EPA 2019 North American Emissions Modeling Platform	(USEPA, 2024b)
Biogenic emissions	BEISv3.6.1/BELD5 driven by GFSv16.2 meteorology	(Vukovich and Pierce, 2002; Schwede et al., 2005)
Wildfire emissions	U.S. EPA 2019 North American Emissions Modeling Platform; Briggs Plume Rise	(USEPA, 2024b; Briggs, 1965)
Other Inline emissions	Sea spray emissions Bi-directional ammonia exchange	(Kelly et al., 2010; Pleim et al., 2013; Gantt et al., 2015; Pleim et al., 2019)

To investigate and quantify the impacts of the in-canopy parameterizations using PA, we run two simulations: 1) "CMAQ-Base" without the canopy effects (hereafter referred to as the "Base" run), and 2) "CMAQ-Canopy" which includes the canopy effects as described above (hereafter referred to as the "Canopy" run). The canopy photolysis and diffusivity parameterizations are simultaneously turned on/off using a single CMAQ model environmental variable flag (i.e., "CTM_CANOPY_SHADE", see updated scripts in code release: https://zenodo.org/records/14502375). For the simulation period, we choose the month of August 01-31, 2019, with 10-days of spin-up (July 22-31, 2019); the spin-up period is discarded and is not included in our analysis. The month of August was chosen because it is a representative warm summer month during both peak contiguous vegetative canopy conditions and high photochemical O_3 formation in the U.S. Thus, choice of this month allows for an ideal investigation of in-canopy photolysis attenuation and vertical turbulence/diffusivity effects on air quality. We select forest locations representing different US forest and ecosystem types for the case study to better understand their differences and canopy impacts on O_3 formation across CONUS (see Section 3 and Table 2 below), in addition to evaluating O_3 across the broader monitoring network. Thus, the choice of this month allows for an ideal investigation of in-canopy photolysis attenuation and vertical turbulence/diffusivity effects on air quality.

The model evaluation includes comparison against observations from the U.S. EPA Air Quality System (AQS) O_3 (Parameter code: 44201) network (https://www.epa.gov/aqs). For the O_3 observational data, 1,217 sites across 48 contiguous U.S. states are paired with modeling data, but only 235 of these sites fall within model grid cells that meet the criteria for a contiguous forest canopy as described above in Section 2.1 (see Section 3.1 and Figure 2 below). We also note that the U.S. AQS observations sites are usually located in urban or suburban areas focused on relatively high population exposure and for public health impacts. Nevertheless, forest canopy processes affecting transported species such as ozone may influence concentrations of those species at locations downwind. As a result, about 19.3% of O_3 sites have canopy effects in the simulations. Consequently, our study compares both the model performance changes for all US

https://doi.org/10.5194/egusphere-2025-485
Preprint. Discussion started: 16 May 2025

346 domain model-observational data pairs (i.e., both “direct” and “indirect” impacts) and canopy
347 effect only model-observation pairs (i.e., “direct” impact).

348

https://doi.org/10.5194/egusphere-2025-485
Preprint. Discussion started: 16 May 2025

3. Results

3.1 Model performance

The Base and Canopy scenarios are evaluated to compare base model performance and demonstrate the impacts of canopy parameterizations (Section 2.2). Figure 2 illustrates the U.S. EPA AQS locations and the regions with vegetative canopy effects applied in the Canopy scenario. The green shaded regions are derived from contiguous canopy thresholds described in Section 2.1. The blue dots indicate AQS locations with direct canopy effects, while the orange dots correspond to grid cells which lack a forest canopy as defined here, and hence are subject to indirect effects. We note that many "indirect effect" grid cells (particularly in Eastern USA) appear within regions surrounded by forest canopies. Nevertheless, these grid cells do not meet the forest canopy selection criteria described above.

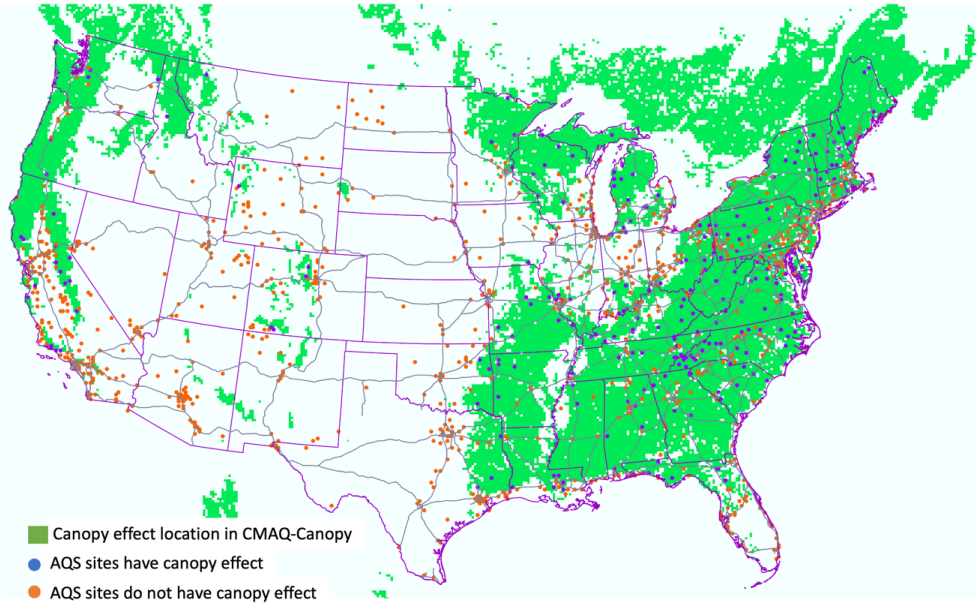

Figure 2. Model domain areas representing the canopy effect regions (green shading) for the Canopy scenario, overlaid with U.S. EPA AQS sites that are both directly (blue dots) and indirectly (orange dots) affected by the vegetative canopy parameterizations. The green shaded regions are derived from contiguous canopy thresholds described in Section 2.1 and generally shown in Figure 1.

Table 2 presents the O_3 performance results (hourly average and Maximum Daily 8-hour average, MDA8) for both model scenarios, including metrics such as data count (number of model-observation pairs used for the analysis) (N), mean bias (MB), mean error (ME), normalized mean bias (NMB), normalized mean error (NME), root-mean-squared error (RMSE), fractional bias (FB), fractional error (FE), and correlation coefficient (R). The mathematical definitions of those performance metrics are in supplementary document. Across all model-observation pairs in the

https://doi.org/10.5194/egusphere-2025-485
Preprint. Discussion started: 16 May 2025

domain, the Base simulation demonstrates good overall performance for O_3 with a MB (NMB) of 0.70 ppb (2.3%), a ME (NME) of 8.49 ppb (27.6%), and a R of 0.75. This performance falls within documented photochemical model benchmark criteria (Emery et al., 2017).

Table 2. Base and Canopy CMAQ model performance for hourly and MDA8 O_3 at all AQS sites and at AQS sites directly affected by canopy. The bold font indicates the improvement caused by canopy effect.

Scenario	AQS location	Data type	N (data count)	MB (ppb)	NMB (%)	ME (ppb)	NME (%)	RMSE (ppb)	FB (%)	FE (%)	R
Base	US Domain	Hourly O_3	885,530	0.70	2.28	8.49	27.6	10.86	9.71	36.1	0.75
Canopy				**-0.10**	**-0.33**	8.49	27.6	**10.89**	**6.37**	36.5	0.75
Base	Canopy effect	Hourly O_3	182,160	2.09	7.48	8.41	30.1	10.7	18.2	40.0	0.73
Canopy				**-1.83**	**-6.58**	**8.24**	**29.5**	**10.6**	**2.41**	40.7	0.73
Base	US Domain	MDA8 O_3	36,510	0.39	0.88	6.72	15.3	8.75	3.1	16.0	0.72
Canopy				**-0.31**	**-0.71**	6.75	15.3	8.77	**1.3**	16.1	0.72
Base	Canopy effect	MDA8 O_3	7,080	1.97	4.9	5.7	14.2	7.36	6.7	14.8	0.73
Canopy				**-1.79**	**-4.5**	5.8	14.5	7.46	**-3.0**	15.1	0.71

The Canopy scenario shows a clear improvement in MB (NMB) for O_3, from 0.7 to -0.1 ppb (2.3 to –0.3 %), and in FB, from 9.7% to 6.4%, across all sites and hence including both direct and indirect canopy effects (Table 2). For sites have canopy effect (blue dots in Figure 2), the Canopy simulation improves most statistical performance measures (MB: 2.09 to -1.83 ppb; ME: 8.41 to 8.24 ppb; RMSE: 10.7 to 10.6; FB: 18.2 to 2.41%) for hourly O_3. While the MB represents the direct average difference between the observational data and the modeled data, the FB represents the difference between normalized observational and modeled data. Because the FB uses normalized differences for each paired prediction, it is less sensitive to the scale of the data (e.g., extremely high, or low values). Consequently, the MB shows an improvement but shifts from a relatively larger overestimation to a smaller underestimation in magnitude (US Domain: 0.7 ppb to -0.1 ppb; Canopy effect location: 2.09 ppb to -1.83 ppb). The FB still indicates that the model tends to overestimate O_3 (US Domain: 9.71% to 6.37%; Canopy effect locations: 18.2% to 2.41%), but the range of overestimation has largely decreased for hourly data in the Canopy run. The MDA8 O_3 for the entire domain has a MB change of 0.39 to -0.31 ppb (NMB is from 0.88 to –0.71%), while the Canopy effect locations have a MB change of 1.97 to -1.79 ppb (NMB is from 4.9% to -4.5 ppb). However, the MDA8 O_3 FB differences are more substantial, with a change of 3.1 to 1.63% for the entire domain, and 6.7% to -3% for canopy effect locations. Thus, according to MB results, the Canopy effect improves the model MDA8 O_3 from slightly overestimated to slightly underestimated, and the FB result shows better improvement in reducing the overall model overestimation. The hourly O_3 concentration distribution, MB, and FB data for the canopy-affected AQS sites are presented in Figure 3. Spatially, the hourly O_3 in the Base scenario is overestimated at nearly all canopy-affected sites in the eastern US (Fig. 3a).

https://doi.org/10.5194/egusphere-2025-485
Preprint. Discussion started: 16 May 2025

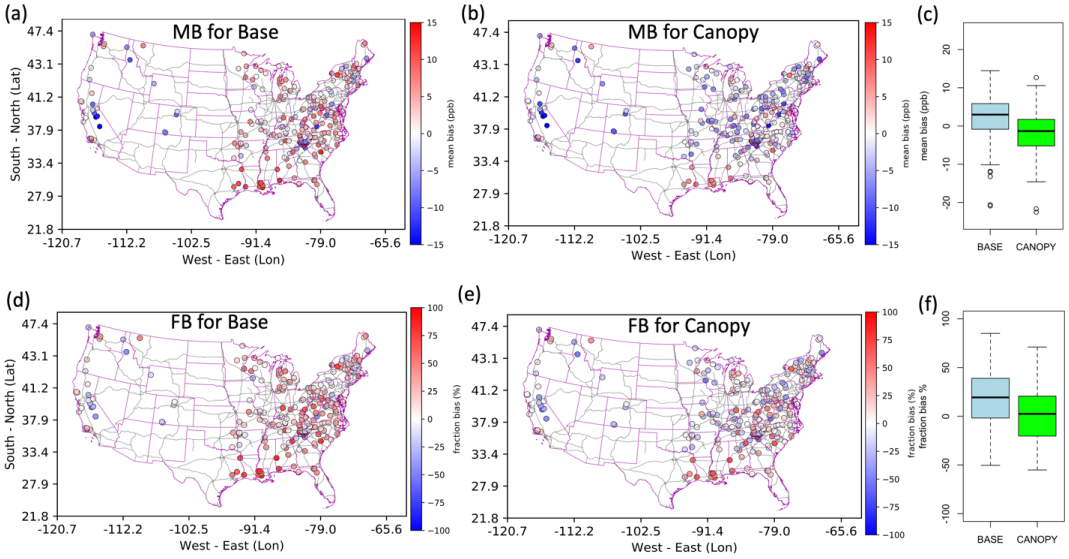

Figure 3. Hourly O_3 mean bias (MB) and fraction bias (FB) spatial plot at AQS sites with direct canopy effects. The upper panels (a, b, and c) are MB for each site; the lower panels (d, e, f) are FB. The (a) and (d) are Base scenarios; (b) and (e) are Canopy scenarios. (c) and (f) are Box-whisker plots (blue = base; green = canopy) for MB and FB at canopy affected AQS sites respectively. The boxes represent the interquartile range (IQR), with the upper and lower lines indicating the 75th (Q3) and 25th (Q1) percentiles, respectively. The thick line in the center of each box represents the median. The circle dots are outliers, defined as values lower than Q1 – 1.5 IQR or higher than Q3 + 1.5 IQR.

Figure 3b shows significant improvement in reducing the O_3 overestimation at direct canopy effect sites with the Canopy scenario, particularly in Mississippi, Alabama, Florida, Arkansas, North Carolina, West Virginia, Virginia, Wisconsin, and Michigan. However, some AQS canopy sites show underestimation in the Base case, which worsens in the sites in Colorado and New York state. The MB values in Fig. 3a and b (N=235) are also represented by a box-whisker plot in Fig. 3c. In the Base case (blue box), around 75% of the canopy AQS sites show overestimation, but the Canopy case demonstrates an improvement in reducing this overestimation. The FB results are shown in the lower panels of Figure 3. The spatial plots in (d) and (e) depict the Base case and the improvement in the Canopy case, respectively, while (f) shows that the range and median FB values for the AQS sites are close to 0% (no bias). Thus, the canopy-affected AQS sites show a clear improvement in reducing overestimation, as indicated by both MB and FB.

Figure 4 shows the improvement in the diurnal pattern of the hourly mean O_3 concentrations for most of the AQS sites affected by the canopy. From 9 to 14 local time, the canopy parameterization has also improved the variability of the model results (compare vertical extent of the observed distributions as white bars to those of the two models; canopy variability is larger than original model and the variability better matches the larger observed variability within these times). The larger variability in the canopy model is impacted by the more discrete nature of the turbulent eddies using Raupach's approach to K diffusivities (Eqs. 2-3).

https://doi.org/10.5194/egusphere-2025-485
Preprint. Discussion started: 16 May 2025

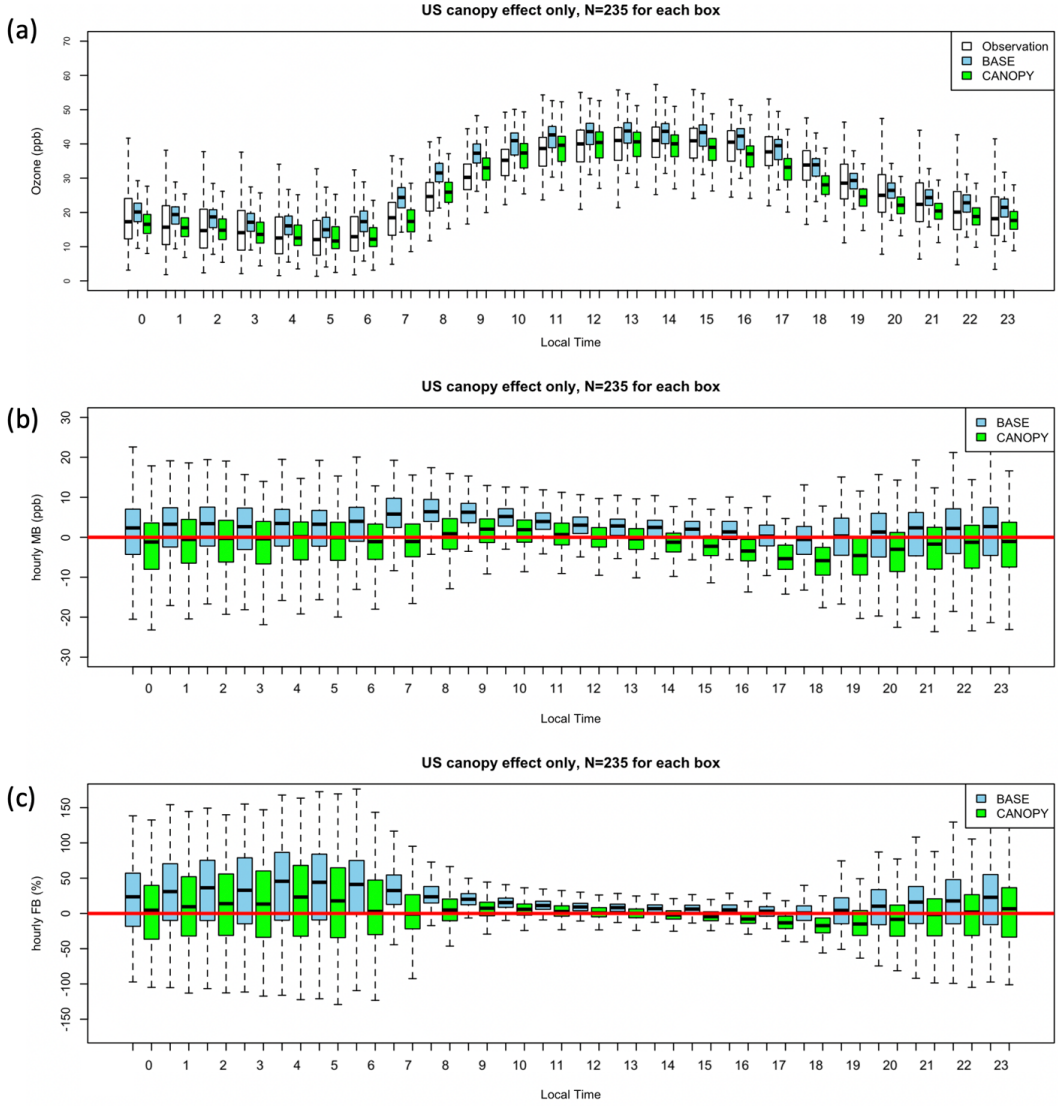

Figure 4. (a) Near-surface (first model layer) diurnal hourly average O_3 concentration (ppb) for canopy-affected AQS sites. Each box represents the monthly hourly average of all AQS sites (235 sites). The white box represents the AQS observations, the blue box is for the BASE case, and the green box is for the Canopy case. (b) Mean bias (MB, in ppb) for the paired data, and (c) Fractional bias (FB, in %) for the same paired data between the AQS observations and the model results. The blue box represents the BASE case, and the green box represents the Canopy case. The bias plots (b and c) show the hourly performance of the model in comparison to the AQS observations.

Diurnally, the BASE model scenarios overestimate O_3 from 12 AM to 5 PM and 9 PM to 11 PM local time (LT), while the Canopy case shows O_3 mean ranges closer to observations (Fig. 4a). For a relatively narrow period of 5 PM to 7 PM LT, however, the Base case performs better,

https://doi.org/10.5194/egusphere-2025-485
Preprint. Discussion started: 16 May 2025

whereas the Canopy case shows a larger underestimation for most AQS sites. Figure 4b represents the MB calculated from paired data, and Figure 4c shows the FB. Figures 4b and 4c illustrate that daytime (8 AM to 4 PM LT) O_3 concentrations are higher (AQS mean Inter-Quartile Range (IQR) is 32 to 42 ppb at 12 PM LT; Base is 38 to 43 ppb; Canopy is 35 to 40 ppb) but exhibit lower bias (Base: IQR of MB is 0.9 to 5 ppb at 12 PM LT; FB is 3.7% to 14%). The Canopy case improves the overestimated O_3 ranges and comes closer to centering the range around the perfect score values (Canopy: IQR of MB is -2.4 to 2.4 ppb at 12 PM LT; FB is -4.8% to 8.3%). Nighttime O_3 concentrations (6 PM to 6 AM LT) are lower (AQS hourly mean IQR is 12.3 to 24 ppb; Base is 17 to 23 ppb; Canopy is 13 to 19 ppb) but have larger bias ranges (BASE: IQR of MB is -4.3 to 7.0 ppb at 12 AM LT; FB is -18% to 57%). The Canopy effect reduces the overestimation seen in the Base case (Canopy: IQR of MB is -8 to 3.6 ppb at 12 AM LT; FB is -36% to 40%), again centering the biases about the zero better than the base case.

The largest improvement due to the canopy effect happens in the morning at 8 AM. The AQS hourly mean IQR is from 20 to 29 ppb at 8 AM LT, the Base case IQR is 29 to 34 ppb, while the Canopy case is much closer at 23 to 29 ppb. The paired data also shows the improvement from Base case (IQR range of MB is from 3.9 to 9.5 ppb at 8 AM LT; FB is from 15 to 38 %) to Canopy case (IQR of MB is from -3.0 to 4.7 ppb at 8 AM LT; FB is from -10 to 20 %). These results illustrate the canopy effect on improving CMAQ's overall diurnal O_3 patterns during both daytime and nighttime, with some degradation with larger underestimations in late afternoon early evening (e.g., 5 to 7 PM LT).

https://doi.org/10.5194/egusphere-2025-485
Preprint. Discussion started: 16 May 2025

3.2 Canopy Impacts on O_3

In regions with direct canopy effects, the canopy parameterizations in CMAQ lead to forest shading and reduced photolysis during the daytime, and reduced transport of O_3 and other titrating molecules during the nighttime (in agreement with Makar et al., 2017). This effectively lowers the near-surface (i.e., first model layer) O_3 diurnal profile in Canopy compared to Base (Figure 4). Overall, the Canopy simulation demonstrates an improved O_3 diurnal profile and reduces overestimation (especially FB) compared to AQS observations. However, direct canopy effects can also exacerbate Base CMAQ underpredictions during some hours of the later afternoon and evening. To provide more insight on this result, the following sections comprehensively analyze, discuss, and quantify the impacts of the canopy parameterizations in the lowest model layers for O_3 and related NO_x processes using CMAQ-PA.

3.2.1 Effects of the canopy on O_3 concentrations in the U.S.

For August 2019, higher monthly average O_3 concentrations in the first (approximately 0-40 m AGL) and second model layers (approximately 40–90 m AGL) are observed in mountainous and suburban areas near Los Angeles, Denver, Salt Lake City, Chicago, Detroit, and New York City (Fig. 5a and 6a). The widespread effects of the canopy parameterizations result in significant reductions in the first model layer monthly average O_3 concentrations for Canopy compared to Base, particularly in the dense forest regions of the eastern U.S., with a maximum grid cell decrease of about 9 ppb (Fig. 5b). However, the canopy effects also lead to increases in the second layer O_3 concentration, with a maximum increase of about 3 ppb (Fig. 6b). Hence, we next use CMAQ-PA to further diagnose and quantify the contrasting canopy impacts on first and second model layer O_3 concentrations.

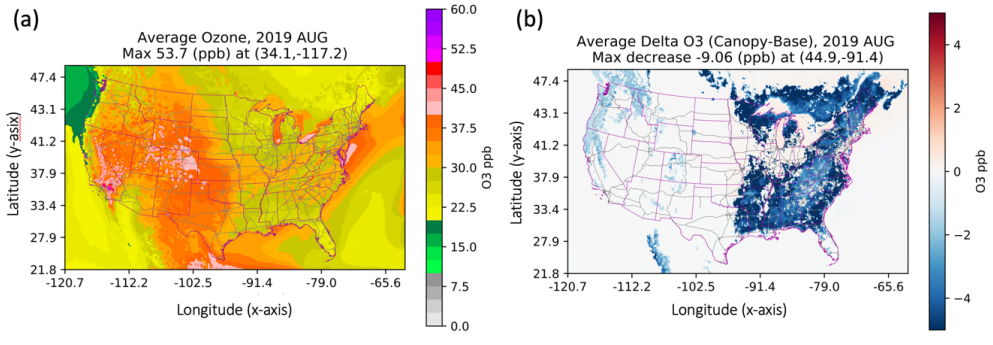

Figure. 5 First layer(0 – 40 m) Base case monthly average O_3 concentration (a) and the monthly average difference (b) between Canopy case and Base case (Canopy - Base) in 2019 August.

https://doi.org/10.5194/egusphere-2025-485
Preprint. Discussion started: 16 May 2025

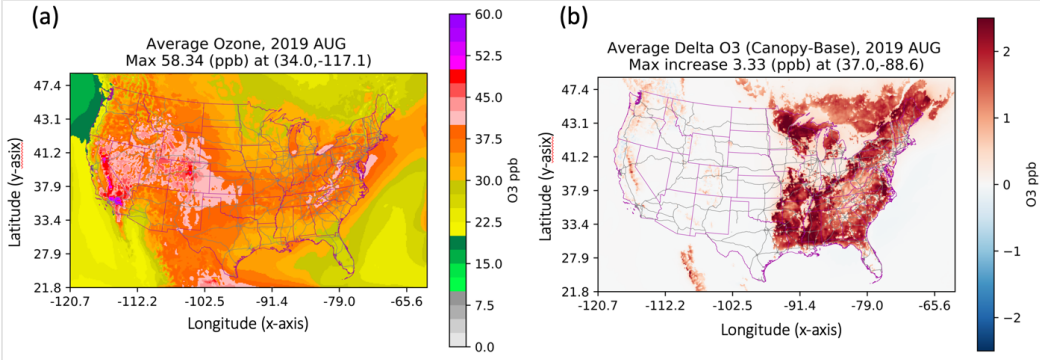

Fig. 6 Second layer (40 – 90 m) Base case monthly O_3 concentration (a) and the difference (b) between Canopy case and Base case (Canopy - Base) in 2019 August.

3.2.2 PA results for canopy-effected modeled first layer (0-40 m) O_3 changes

The direct canopy effect locations, shown as green shaded areas in Figure 2, are selected for studying O_3 changes using CMAQ PA output. We also applied a time zone mask for selecting the eastern standard time (EST) region to provide emphasis of the eastern U.S. and thus inherently reducing impacts from the western mountainous regions. To investigate the diurnal patterns for processing rates, the PA data are calculated as one-month averages for each hour and canopy-effected grid cell. The major processes that contribute to O_3 changes are vertical diffusion rate ("v diffusion", green lines), deposition rate (orange lines), and chemical processing rate (red lines) in the morning (Figure 7a).

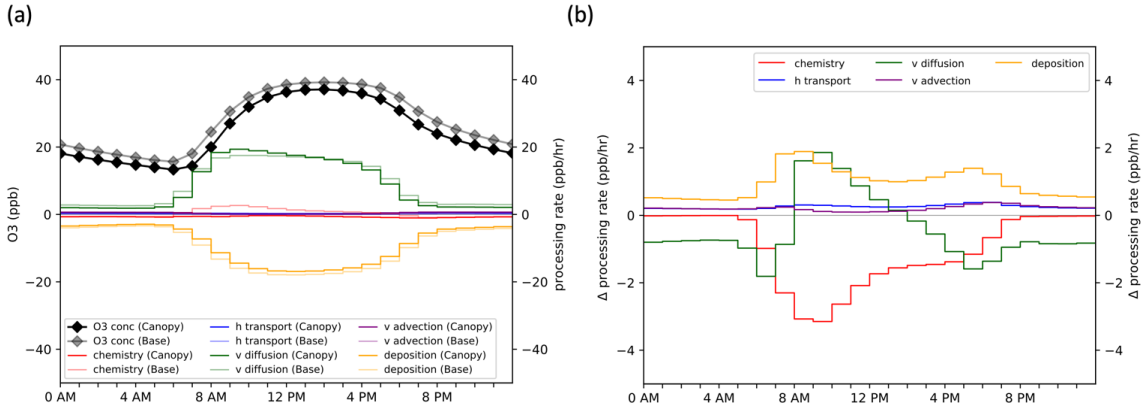

Fig. 7 Hourly average near-surface O_3 (0 – 40 m above surface) process analysis result at Canopy effect locations in August 2019 for (a) two scenarios (Canopy: solid shade, Base: transparent shade) and their process rate differences (Canopy - Base) in (b).

https://doi.org/10.5194/egusphere-2025-485
Preprint. Discussion started: 16 May 2025

The Base case (transparent shaded lines in Figure 7a) shows that vertical diffusion processing rates (transparent green line) contribute significantly to near-surface O_3 concentrations, with a maximum of 18 ppb hr^{-1} at 9–10 AM. Deposition causes the major loss, with a maximum of 18 ppb hr^{-1} at 12–1 PM. The chemical production rate of O_3 (transparent red line) reaches a maximum of 3 ppb hr^{-1} at 9–10 AM during the daytime but becomes negative during the nighttime (7 PM–5 AM). These results indicate that surface O_3 changes in the Base case originate from exchange of O_3 with the upper troposphere, near-surface O_3 chemical production and loss, and loss via deposition to the surface.

In the Canopy case (solid shaded lines in Figure 7a), the daytime maximum near-surface O_3 chemical production rate (red line) becomes all negative (maximum: -1 ppb hr^{-1}) compared to the Base case. This suggests net chemical loss of O_3 within the canopy, where the chemical processing rate difference reaches a maximum of -3 ppb hr^{-1} at 9 AM (Figure 7b). The reduction in chemical processing rate is caused by decreased NO_2 photolysis resulting in less $O(^3P)$ formation and hence less O_3 formation, while at the same locations, the relative amount of NO_x that remains as NO increases due to trapping of fresh emissions, and hence the O_3 titration rate increases, leading to increased O_3 destruction. The net result is a shift from net chemical production to net loss of near-surface O_3, in areas of contiguous canopies.

Additionally, there is a reduction in vertical transport rates due to the impact of contiguous canopies on modulating the eddy diffusivity rates in the lowest model layer (Figure 7b). It is important to note that the quantities depicted in Figure 7(b) are the differences in the rates of change between the two simulations; a negative value indicates that the rate of change has decreased with the canopy parameterization, a positive value indicating that the rate of change has increased. A negative value for the vertical diffusion component (Fig. 7b, green line) thus indicates that the rate of change associated with vertical diffusion has become *more* negative, but not necessarily that the rate of change associated with transport *is* negative, in either simulation.

The vertical diffusion processing rate (Fig. 7b, green line) differences for CMAQ (Canopy-Base) in the first model layer are negative starting in the afternoon (2 PM) and through nighttime into the early morning (5–8 AM LT) by up to -1.8 ppb hr^{-1}. This is due to canopy impacts on relatively less diffusion of higher O_3 concentrations downward in conjunction with chemical net loss of O_3 (from shading and reduced photolysis in mid-afternoon and early morning) in the first model layer (red line). Consequently, the Canopy case develops a la7rger vertical O_3 concentration gradient between the first and second model layers from 7 PM – 7 AM (see Fig. 8 and Fig. S1 for O_3 vertical profile and PBL height).

We note that the rate of change of O_3 due to vertical diffusion can be expressed as:

$$\frac{\partial[O_3]}{\partial t} = -\left\{\frac{\partial K}{\partial z}\frac{\partial[O_3]}{\partial z} + K\frac{\partial^2[O_3]}{\partial z^2}\right\} \quad \text{Eq. 4}$$

https://doi.org/10.5194/egusphere-2025-485
Preprint. Discussion started: 16 May 2025

From Fig. 8 (and Fig. S2), it can be seen that $\partial^2[O_3]/\partial z^2$ is always greater at the second model layer with the use of the canopy parameterization, though weaker above layer 2, and in the early morning, $\partial[O_3]/\partial z$ is less with the canopy model above layer 2, and greater below layer 2, and by the late morning the vertical gradients above the lowest model layer are relatively unchanged. That is, the effects are strongest and extend into the first three layers when the magnitude of K is relatively low (nighttime and early morning). By late morning, with the diurnal increase of K, the canopy affects only be seen in the lowest model layer.

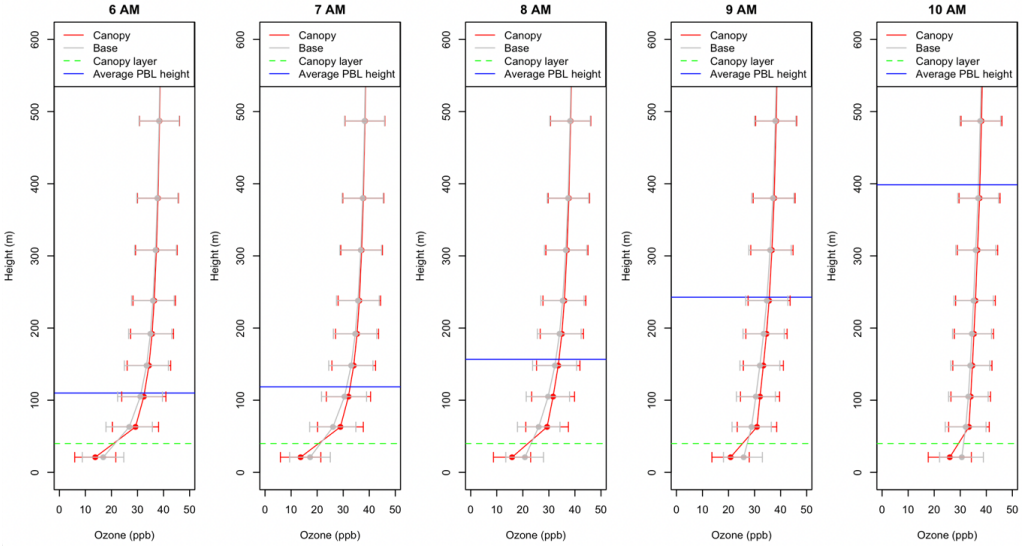

Fig. 8 The hourly vertical O_3 profiles of Base (gray) and Canopy (red) at 6 AM to 10 AM LT. The dots in each layer are average O_3 concentration in regions of canopy effects in Fig. 2 and the range bars are the standard deviation range. The blue Line is the hourly average PBL height, and the green dash line is the forest canopy height.

At 8 AM, the average planetary boundary layer (PBL) height increases to 160 m AGL (higher than the fourth layer), in response to morning increases in the magnitude of K, which allows for more O_3 that had previously built up in the free troposphere transport downward into the PBL (Fig. 8). This results in increases to the vertical diffusion O_3 processing rate of about 1.5 – 2 ppb hr^{-1} for the canopy compared to Base case between 8 AM – 2 PM in the first model layer (Figure 7b). In other words, the presence of the canopy via the modified K profile delays the downward transport of higher O_3 aloft (due to buildup during late afternoon, evening, and early morning) until the PBLH grows high enough into the region where the canopy increased gradient dissipates after 8 AM LT. Therefore, the first model layer O_3 changes due to the canopy (i.e., net decrease all hours; see black lines in Figure 7a) is caused by both decreased photolysis and modulated vertical diffusion processes. The reduction of near-surface O_3 concentration also reduces the deposition rate (Fig. 7a from -14 to -12 ppb hr^{-1} at 8 AM LT).

https://doi.org/10.5194/egusphere-2025-485
Preprint. Discussion started: 16 May 2025

3.2.3 PA results for canopy-effected modeled second layer (40 - 90 m AGL) O_3 changes

Unlike the first (lowest) model layer (0 – 40 m AGL) that always has positive O_3 vertical transport process (upper layer O_3 are transported to surface by diffusion), the second layer vertical transport processes in the Base run (Fig. 9a, diffusion, green transparent line) only shows positive in the morning hours of 8 AM to 11 AM LT. Figure 9a is presented in duo y-axis, the left y-axis is concentration, and the right y-axis is processing rate.

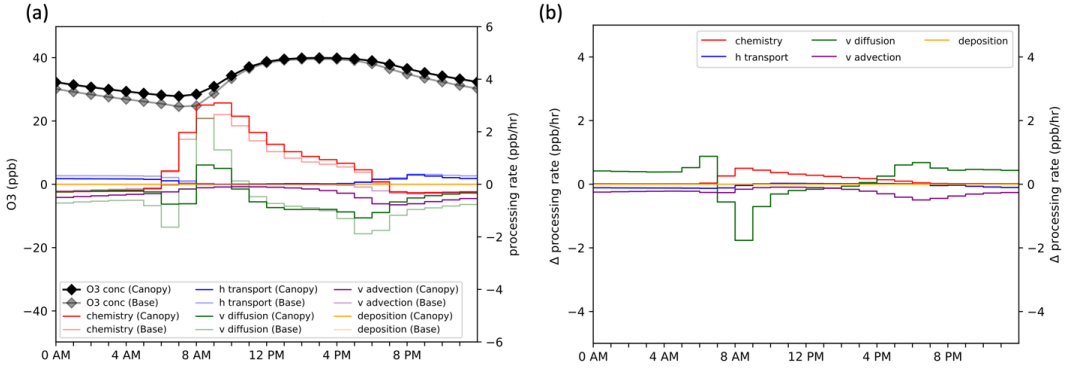

Fig. 9 Hourly average 2nd layer (40 – 80 m above surface) O_3 process analysis result at Canopy effect locations in August 2019 for (a) two scenarios (CMAQ-Canopy: solid color, CMAQ-Base: transparent color) and their differences (Canopy - Base) in (b).

From midnight to early morning (0 AM to 6 AM LT), the loss of second layer O_3 transported downward (v diffusion) to the first model layer is reduced due to the canopy (transparent green line to solid green line). At 6 AM LT (sunrise), the PBL height is above the second model layer height at roughly 110 m (close to the third model layer height; Fig 8), and the chemical O_3 formation process has become positive (Fig. 9a; Base: 0.47 ppb hr^{-1}, Canopy: 0.5 ppb hr^{-1}). At 7–8AM LT, the increase of O_3 concentration gradient (~15 ppb between first and second model layer) further demonstrates the one-hour delay in vertical diffusion from the second layer down to the first model layer (see Fig9a, green line at 6–8 AM). This emphasizes the effect of the canopy in building up O_3 concentrations in the second model layer over the late afternoon, evening, and early morning hours (Fig. 9b; positive net O_3 difference, green line) that also sharpens the concentration gradient between the first and second model layers during these hours.

During the morning hours (8 AM to 11 AM LT), the PBL height is above the fourth model layer and there is a smaller concentration gradient between the third layer and the second layer in the Canopy case compared to Base (Fig. 8). Hence, there is relatively less O_3 transport from the third layer into the second model layer due to the canopy (Figure 9a, green lines; 8 AM to 11 AM LT). In the afternoon hours of 12 PM to 4 PM LT, the PBL height grows higher, and O_3

https://doi.org/10.5194/egusphere-2025-485
Preprint. Discussion started: 16 May 2025

concentration reaches an equilibrium state between the third and second layers (Fig. S2), resulting in minimum diffusion transport from the third to the second layer. Although there is almost no O_3 transport from the third to the second layer, the additional chemical formation of O_3 in the second layer (due to canopy-imparted NO_x changes; see Section 3.2.4) increases O_3 concentrations and resulting transport to the first model layer, as reflected in the increased vertical transport (diffusion and advection) loss processing rate (green and purple line; Figure 9b at 12 PM to 4 PM LT). At nighttime between 8 PM to 5 AM LT, there is no new O_3 formation (rather destruction) in the second layer, while the canopy effect reduces O_3 diffusion loss from the second layer to the surface layer (green and transparent green lines; Fig. 9a) but increase the O_3 advection loss from second layer the surface layer (purple and transparent purple lines; Fig. 9a). Considering summation of all vertical process, the diffusion process is still larger than advection process. This further reemphasizes that as a result, the O_3 concentration in the second layer is higher at night in the Canopy run.

The chemical processing rate contributes substantially to O_3 concentration during photochemical daytime hours (6 AM to 6 PM) in the second model layer (transparent and solid red lines in Figure 9a). In the Canopy case (solid red line), the O_3 chemical processing rate increases during all daytime hours compared to the Base case, maximizing at about 0.5 ppb hr^{-1}at about 8–9 AM. To investigate the reasons leading to the chemically induced O_3 increase in the second layer for the Canopy case, we investigate the NO_x PA in the first model layer, which is the closest model layer to major NO_x emission sources at the surface.

3.2.4 PA results for canopy-effected modeled NO_x

Figure 10 shows the first layer NO_x concentration and total processing rates (10a for NO_x, 10d for NO, and 10g for NO_2), explicit processing rates results (10b for NO_x, 10e for NO, and 10h for NO_2), and delta processing rates (Canopy- Base) (10c for NO_x, 10f for NO, and 10i for NO). In Fig.10 first row, the canopy leads to increases in NO_x concentrations in the first model layer (Fig. 10a; month average difference: +0.16 ppb, +13.6%), and the PA results show that the increase is caused by the reduction of vertical transport loss from the first to second model layer (Fig. 10b; transparent and solid green lines, maximum difference at 6AM, -0.02 ppb hr^{-1}) and reduction of chemical loss at 7 AM to 7 PM. (Fig. 10b; transparent and solid red lines, maximum difference at 8 AM, -0.05 ppb hr^{-1}). The section 3.3 explains the details of NO_x chemical reaction changed. For other processing rate of NO_x, the horizontal transport (blue line) and vertical advection (purple line) of NO_x are nearly identical between the two simulations, and hence the change in horizontal transport and vertical advection are minimal (Fig. 10c).

Figure 10 second row presents the NO PA results. Most NO sources in the first model layer are due to surface emissions, with a monthly average rate of 0.95 ppb hr^{-1} (Fig. 10e, magenta line). The Canopy case reduce the vertical diffusion loss (i.e., more trapping) of NO from the first to second model layer, with a maximum difference at 9 AM of +1.1 ppb hr^{-1} (Fig. 10f; solid green

https://doi.org/10.5194/egusphere-2025-485
Preprint. Discussion started: 16 May 2025

lines). This inherently leads to an increase in the NO chemical loss rate of via various chemical processing pathways (e.g., NO + O_3, HO_2, or $RO_2 \rightarrow NO_2$, see shift from Base transparent red line to Canopy solid red line; Figure 10e and delta processing red line in Figure 10f).

The maximum delta NO chemical loss (-1.0 ppb hr^{-1}) occurs at 9 AM, which is coincident with the increase in NO_2 concentration (Fig. 10 third row, panel g, monthly average difference: +0.2 ppb). This relative decrease (increase) in NO (NO_2) is attributed to both canopy shading/reduced photolysis ($NO_2 \rightarrow NO$) and enhanced chemical formation ($NO \rightarrow NO_2$,), as represented by the red line in Fig. 10h. The Fig. 10i show the changes of NO_2 processing rates. The peak NO_2 chemical formation occurred at 9 AM (1.1 ppb hr^{-1}), coinciding with the maximum difference in vertical transport loss at 9 AM (-1.1 ppb hr^{-1}) along with the maximum of the emissions offset in NO (which is rapidly transformed to NO_2 via the reactions noted above). With higher source NO emissions in the morning up to 9 AM, and stronger vertical mixing facilitated by deeper PBL heights during the morning hours after 9 AM, the additional NO_2 due to canopy effects transported from the first to the second layer increases the NO_2 photolysis rate in the second layer during daylight hours (particularly between 8 AM and 5 PM, Fig. S3h). This process enhances the chemical production of O_3 in the second layer (Fig. 9a; red lines). Meanwhile, the canopy-impacted NO in the first layer results in less transport to the second layer, decreasing the NO titration rate in the second layer and thereby increasing O_3 concentrations here as well. These chemical and physical processes shift the NO-to-NO_2 mixing ratio in terms of average vertical transport loss in the first model layer: from 51% : 49% in the Base case (average daily total: 20.4 ppb) to 16% : 84% in the Canopy case (average daily total: 19.2 ppb).

The second layer O_3 PA results further confirm these chemical and transport changes between the first and second model layers (Fig. S3). The reduced vertical transport in the lowest model layer results in more conversion of NO to NO_2 there, with the result that relatively more NO_2 is transported upwards from the first layer with the canopy model. When this NO_2 emerges into layer 2 (mostly above the canopy, at higher light levels), it photolyzes, leading to an increase in layer 2 in O_3 production. More NO_x is trapped in the first model layer by Canopy (and in the darker environment, more of this NO_x is converted to NO_2 and not photolyzed back to NO) NO_x concentrations are inherently reduced in second layer (Figure S3a), though the proportion of NO_x which is NO_2 has increased, especially in the early morning (5AM – 8 AM). When the enhanced NO_2 is transported from surface to the second layer later in the morning and early afternoon, it increases the second layer NO_2 vertical transport process (Fig. S3i, green line, max: +0.5 ppb hr^{-1} at 8 AM), enhances daytime NO_2 photolysis to NO and generates more O_3 (Fig. S3i, red line, max: -0.4 ppb hr^{-1} at 8 AM).

https://doi.org/10.5194/egusphere-2025-485
Preprint. Discussion started: 16 May 2025

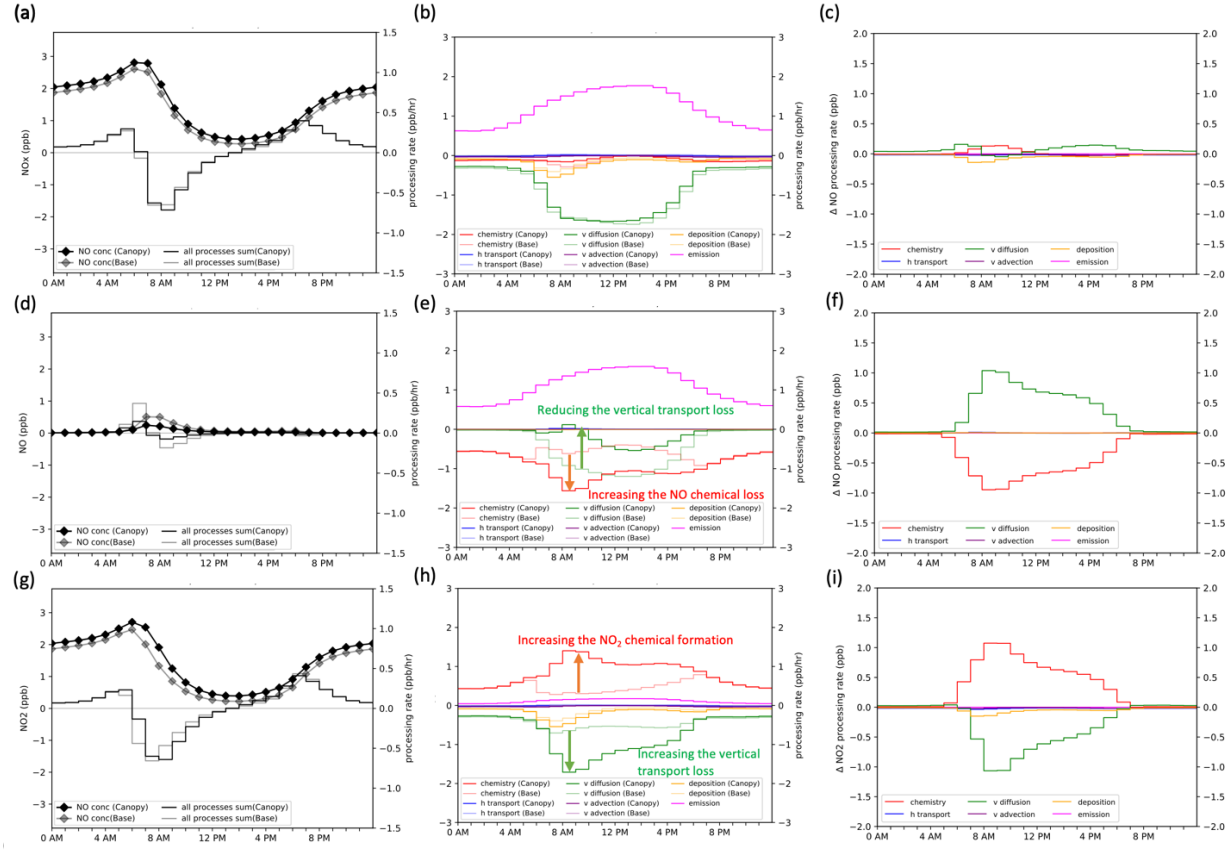

659 Fig. 10 Hourly average surface layer (0 - 40 m AGL) process analysis result for (a) NO_x concentration and net
660 process; (b) NO_x explicit processing rates; (c) delta (Canopy- Base) NO_x processing rate (d) is NO concentration
661 and net process; (e) is NO explicit processing rates; (f) delta (Canopy- Base) NO processing rate (g) is NO_2
662 concentration and net process; (h) is NO_2 explicit processing rate and (i) delta (Canopy- Base) NO_2 processing rates
663 at Canopy effect locations in August 2019 for two scenarios (Canopy and Base).
664

https://doi.org/10.5194/egusphere-2025-485
Preprint. Discussion started: 16 May 2025

3.3. Process Analysis and Integrated Reaction Rate result summary for O_3, NO_x and VOC reactions

Overall, the daily total canopy runs result in net reductions of first model layer O_3 chemical formation rates (-21 ppb d^{-1}, -303%) and vertical transport rate (-5 ppb d^{-1}, -2.3%). The canopy leads to increases in chemical formation rates (2.9 ppb d^{-1}, +24.8%) in the second model layer (Table 3). The canopy results in large reductions in photolysis, less $NO_2 \rightarrow NO$ conversion, enhanced NO transformation to NO_2 in the first model layer, and consequently more NO_2 transported into the second layer during daytime hours. This process increases the second layer O_3 production rates (+ 1.5 ppb d^{-1}) and reduces O_3 consumption rates (- 1.4 ppb d^{-1}). These two factors cause the net second layer O_3 monthly average chemical processing rate to increase of 2.9 ppb hr^{-1} (+24.8%). Table S1 in the supplementary document shows the daytime (6 AM to 6 PM LT) and nighttime (6 PM to 6 AM LT) O_3 process rate details.

Table 4 shows the NO_x processing rates and IRR results for the first and second layers to help explain the O_3 chemical process changes. The first model layer NO_x chemical processing shows that the total NO to NO_2 process increases by about 22.1 ppb (31.2%). The changes of NO reaction processes due to the canopy include a net 1) increase in the NO + O_3 reaction from 41.5 to 78.5 ppb (+89.2%), 2) decrease in NO + RO_2 reaction from 29.1 to 14.2 ppb (-51.2%), and 3) decrease in the NO_2 photolysis process ($NO_2 \rightarrow O + NO$) from 95.6 to 36.2 ppb (-62.1%). Hence, the NO_x cycle was changed and overall net O_3 chemical processes become negative in the first model layer (Table 3; from 6.9 to -14 ppb, -302.9%). This results in an increase in the first model layer NO_2 vertical transport loss (from -9.9 to -16.1 ppb, +62.6%) and decreases the NO vertical transport loss (from -10.5 to -3.1 ppb d^{-1}, -70.5%). Further, due to reasons described above, the second layer NO_x chemical processes have an increase in NO_2 photolysis rate (from 86 to 87.8 ppb d^{-1}, +2.1%) and decreasing NO titration (NO + O_3) reaction (from 65.9 to 64.8 ppb d^{-1}, -1.7%). Those NO_x balance changes cause the net chemical O_3 formation to increase about 2.9 ppb d^{-1} in the second model layer (+24.8%).

In addition to the changes in the NO_x cycle caused by the canopy, the HO_x radicals (OH and HO_2) and VOC oxidation processes are significantly impacted. Table 5 summarizes the effects of the canopy on HO_x formation and VOC oxidation reactions, focusing on changes in the Integrated Reaction Rate (IRR) driven by canopy influence. The sources of "new" HO_x radicals include inorganic source (e.g., $O(^1D) + H_2O$) and organic sources (e.g., photolysis of aldehyde compounds). The canopy reduces both photolysis processes, the photolysis of O_3 ($O_3 \rightarrow O(^1D)$, decreased by 75.8%) and formaldehyde (FORM $\rightarrow 2HO_2$, decreased by 74.3%). These reductions greatly diminish OH radical formation and result in a 49.6% decrease in VOC + OH reactions. Fewer OH radicals lead to reduced VOC oxidation, resulting in lower RO_2 and HO_2 formation. Consequently, the reactions between NO and RO_2 or HO_2 decrease by 51% (Table 4). The sharp decline in OH radical formation also limits net NO_z (HNO_3 and HONO) formation processes (-45%) in table 4,

https://doi.org/10.5194/egusphere-2025-485
Preprint. Discussion started: 16 May 2025

such as $NO_2 + OH \rightarrow HNO_3$ and $NO + OH \rightarrow HONO$, which reduces the chemical loss of NO_x in the first layer, as indicated by the red line in Fig. 10b and 10c.

While VOC + OH reactions experience a significant reduction (-49.6%) in Table 5, VOC oxidation reactions with O_3 in the first layer shows an increase (+36.5%), with reaction rates rising by 1.48 ppb d^{-1}. This increase is attributed to the reduced OH radical levels and O_3 photolysis rate in the first layer, which create more opportunities for VOCs to react with O_3. Notable increases are observed in isoprene (from 0.56 to 1.23 ppb d^{-1}, + 120%), monoterpenes (from 1.18 to 1.48 ppb d^{-1}, + 25.4%), and other alkenes (from 2 to 2.51 ppb d^{-1}, +25.5%) (see table S2). In the second layer, changes remain minimal, only VOC + OH reactions increase slightly by 7.4%, +0.9 ppb d^{-1}. The changes in VOC + NO_3 reactions are also negligible, with rate changes contribution is below 3% (0.18 of 6.0 ppb d^{-1}) in first layer and 0.7% (0.006 of 0.95 ppb d^{-1}) in second layer. This chemistry and advection-driven pooling of biogenic VOCs within the canopy has been seen in observations and in high resolution 1-D canopy models in the past (Makar et al., 1999); differences in reactivity of the VOCs can lead to underestimates of the most reactive VOCs relative to those generated in the absence of chemical losses with the “big-leaf” model framework.

https://doi.org/10.5194/egusphere-2025-485
Preprint. Discussion started: 16 May 2025

Table 3 First and Second layer O_3 PA results for Base and Canopy scenario one-month average daily total processing rates.

layer	O_3 process	Base (ppb d^{-1})	Canopy (ppb d^{-1})	Difference (ppb d^{-1})	Difference (%)
First Model layer	O_3 vertical transport	213	208	-5	-2.3%
	O_3 horizontal transport	3.67	9.61	5.94	161.9%
	O_3 deposition	-224	-203	21	-9.4%
	net chemical O_3 process	**6.9**	**-14**	**-20.9**	**-302.9%**
	O_3 chemical production	673	167	-506	-75.2%
	O_3 chemical reduction	666	181	-485	-72.8%
Second Model layer	O_3 vertical transport	-17	-19.2	-2.2	12.9%
	O_3 horizontal transport	4.41	3.43	-0.98	-22.2%
	O_3 deposition	0	0	0	0%
	net chemical O_3 process	**11.7**	**14.6**	**2.9**	**24.8%**
	O_3 chemical production	677.7	679.2	1.5	0.2%
	O_3 chemical reduction	666	664.6	-1.4	-0.2%

Table 4 The average daily total NO_x chemical cycle process, and net all processing rates on surface and second layer at canopy effect regions (see Figure 2).

Layer	Processing description	Target species or reactions	Base (ppb d^{-1})	Canopy (ppb d^{-1})	Difference (ppb d^{-1})	Difference (%)
First Model layer	Emission	NO_x	26	26	0	0.0%
		NO	23.7	23.7	0	0.0%
		NO_2	2.37	2.37	0	0.0%
	Vertical Transport	NO_x	-20.4	-19.2	1.2	5.90%
		NO	-10.5	-3.1	7.4	-70.5%
		NO_2	-9.9	-16.1	-6.2	62.6%
	Horizontal Transport	NO_x	0.13	-0.29	-0.42	-323%
		NO	0.097	0.099	0.002	2.10%
		NO_2	0.035	-0.39	-0.425	-1,214%
	Deposition	NO_x	-2.66	-3.49	-0.83	31.2%
		NO	-0.071	-0.054	0.017	23.9%
		NO_2	-2.59	-3.44	-0.85	32.7%
	Chemical process	**Total NO → NO_2**	**70.6**	**92.7**	**22.1**	**31.3%**
		NO + O_3 → NO_2	**41.5**	**78.5**	**37**	**89.2%**
		NO + HO_2 or RO_2 → NO_2	**29.1**	**14.2**	**-14.9**	**-51.2%**
		NO_2 → NO+O	**95.6**	**36.2**	**-59.4**	**-62.1%**
		Net NO_x → NO_z	**0.65**	**0.36**	**-0.29**	**-44.6**
Second Layer	Emission	NO_x	2.08	2.08	0	0.0%
		NO	1.87	1.87	0	0.0%
		NO_2	0.2	0.2	0	0.0%
	Vertical Transport	NO_x	-0.14	-0.16	-0.02	14.3%
		NO	1.51	-0.43	-1.94	-129%
		NO_2	-1.65	0.28	1.93	-117%
	Horizontal Transport	NO_x	0.41	0.32	-0.09	-22.9%
		NO	0.11	0.13	0.02	18.2%
		NO_2	0.2	0.28	0.08	40.0%
	Deposition	NO_x	0	0	0	0.0%
		NO	0	0	0	0.0%
		NO_2	0	0	0	0.0%
	Chemical process	Total NO → NO_2	88.9	88.82	-0.04	0.0%
		NO + O_3 → NO_2	**65.9**	**64.8**	**-1.1**	**-1.70%**
		NO + HO_2 or RO_2 → NO_2	23.0	24.02	1.06	4.60%
		NO_2 → NO+O	**86.0**	**87.79**	**1.8**	**2.10%**
		Net NO_x → NO_z	0.55	0.53	-0.02	-3.6%

https://doi.org/10.5194/egusphere-2025-485
Preprint. Discussion started: 16 May 2025

Table 5 The average daily total IRR results of new HO_x (OH and HO_2) and VOC oxidation reactions on surface and second layer at canopy effect regions (see Figure 2).

Layer	Processing description	Reaction Number &	Target species or reaction	Base (ppb d^{-1})	Canopy (ppb d^{-1})	Difference (ppb d^{-1})	Difference (%)
First Model layer	Inorganic source of HO_x	R9	$O(^1D)$ production from O_3 photolyzed	30.4	7.37	-23.03	-75.8%
		R11	$O(^1D) + H_2O$	3.03	0.72	-2.31	-76.4%
	Organic source of HO_x	R97	FORM photolyzed	1.34	0.35	-1.00	-74.3%
		R108	ALD2 photolyzed	0.08	0.02	-0.06	-75.0%
	Total New HO_x radicals	R11, R97, R108	New HO_x from O1D, FORM, and ALD2	8.73	2.12	-6.61	-75.7%
	VOC oxidation reactions	#	VOC + OH	15.1	7.61	-7.49	-49.6%
		$	VOC + O_3	4.05	5.53	1.48	36.5%
		%	VOC + NO_3	0.57	0.75	0.18	31.6%
Second Model layer	Inorganic source of HO_x	R9	$O(^1D)$ production from O_3 photolyzed	30.8	30.7	-0.1	-0.3%
		R11	$O(^1D)$ + H2O	3.03	3.05	0.015	0.5%
	Organic source of HO_x	R97	FORM photolyzed	1.36	1.43	0.07	5.2%
		R108	ALD2 photolyzed	0.08	0.08	0.003	3.8%
	Total New HO_x radicals	R11, R97, R108	New HO_x from O1D, FORM, and ALD2	8.77	8.94	0.17	1.9%
	VOC oxidation reactions	#	VOC + OH	12.1	13	0.9	7.4%
		$	VOC + O_3	2.35	2.4	0.05	2.13%
		%	VOC + NO_3	0.587	0.593	0.006	1.0%

& CB6r3 Reaction Number reference can be found: https://github.com/USEPA/CMAQ/blob/main/CCTM/src/MECHS/cb6r3_ae7_aq/mech_cb6r3_ae7_aq.def

VOC+OH reactions include: R106, R110, R113, R116, R121, R_125, R126, R127, R130, R131, R132, R138, R142, R146, R149, R158, R165, R170, R172, R180, R185, R186, R191, R199, R203, R206

$ VOC + O_3 reactions include: R139, R143, R147, R156, R159, R173, R200, R204

% VOC + NO_3 reactions include: R107, R111, R115, R118, R120, R140, R144, R148, R157, R160, R164, R174, R192, R201, R205, R207

https://doi.org/10.5194/egusphere-2025-485
Preprint. Discussion started: 16 May 2025

4. Conclusion and Discussion

In this work, we implemented explicit vegetative canopy data and efficient parameterizations (Eqs. 1-3 above following Makar et al., 2017) for the effects of forest shading on photolysis attenuation and canopy-modulated turbulence (i.e., eddy diffusivities) into the widely used CMAQ model. We adopted a simplified approach, which implements the parameterization within CMAQ's existing layer structure, rather than locally adding additional layers explicitly into canopy grid cells, by weighting the sub vertical grid scale photolysis rates and diffusivities by reduction factors to account for the light and turbulence structure within the canopy portion of the model layers. We comprehensively analyzed and quantified the impacts of the canopy data and parameterizations on boundary layer O_3 predictions using CMAQ-Process Analysis (CMAQ-PA). To our knowledge, this work using the PA method is the first to detail and quantify the different roles of dynamics, physical, and chemical processes due to the presence of forest canopies on O_3.

Overall, the O_3 concentration is directly impacted at the canopy effect locations in the model. The canopy effect improves the model performance (mean bias from +0.70 ppb to −0.10 ppb and fractional bias from +9.71% to +6.37%) for hourly O_3, especially in the morning hours (e.g., 7–11 AM LT). The PA results show substantial changes in the O_3 chemical process rate, both in sign and magnitude (net chemical process from +6.9 ppb d^{-1} to -14 ppb d^{-1}, a –303% change), while also altering the gas chemistry and partitioning of other NO_x, HO_x, and VOC oxidation reactions. The canopy leads to strong reductions in the photolysis of NO_2, O_3 and formaldehyde in the first model layer, which not only decreases the NO_2 photolysis rate (-62.1%) but also significantly reduces the OH radical formation rate (-75%) from both inorganic ($O(^1D)$) and organic (formaldehyde) pathways. These changes result in a -49.6% decrease in OH-initiated VOC oxidation reactions, while increasing the VOC + O_3 reactions (+36.5%). Furthermore, enhanced trapping NO_x and the conversion of NO to NO_2 by the canopy in the first model layer consequently leads to higher NO_2 photolysis and lower NO titration in the second layer. This causes an overall increase in net O_3 daily total chemical processing rate in the second layer (monthly average ~ 2.9 ppb d^{-1} or +24%).

Altered O_3 concentration gradients due to the canopy (e.g., increased gradient between first and second but decreased gradient between second and third layers) leads to an enhanced, but delayed (between about 6-8 a.m.) effect of downward transport of ozone from the second to the first model layer. Overall, the complex chemical and physical diffusion processes induced by the canopy effect reduce first layer (near-surface) O_3 concentrations (see black lines in Figure 7a), while increasing O_3 concentrations in the subsequent layers above, and most predominantly during the nighttime through morning hours in the second layer (see black lines in Figure 9a).

Our results of the impacts of sub-canopy parameterizations in CMAQ compare well with past work implementing a similar, but more explicit multi-sublayer methodology in the Global

https://doi.org/10.5194/egusphere-2025-485
Preprint. Discussion started: 16 May 2025

Environmental Multiscale-Modeling Air quality and CHemistry (GEM-MACH) model (Makar et al., 2017). Both our parameterizations and the work of Makar et al. (2017) show a similar reduction of the mean bias (MB) of more than 50% compared to near-surface, CONUS-wide O_3 observations. Our work, however, further emphasizes the differences between CONUS-wide and "canopy-effect" locations, as well as the even larger impact of the canopy on near-surface O_3 fractional biases (FB), which representing the difference between normalized observational and modeled data (i.e., less sensitive to scale or range in data values).

There are, however, some inherent uncertainties in this study that can be addressed in the future. Notably, the impacts of the canopy parameterizations are dampened by the relatively coarse thickness of the first model layer (~40m) in the CMAQ configuration employed (Section 2.3), which is consistently larger (significantly in some cases) than forest canopy heights across the U.S. (Figure 1). This dilutes the in-canopy photolysis and diffusivity effects when integrated to obtain a "best value" within the first layer of the meteorological model layer structure currently resolved by our CMAQ implementation. In the future, the use of the multi-sublayer method (Makar et al., 2017) to improve vertical resolution could better reflect the details of the vertical structure of the canopy and further improve predictions of O_3 in CMAQ.

Nevertheless, the implementation here shows that relatively simple sub-canopy parameterizations for canopy shading and turbulence lead to improvements in CMAQ's O_3 performance, underscoring the importance of including these processes and supporting canopy data in CTMs to improve predictions of regional ozone chemistry. Further quantifying the effects of these sub-canopy parameterizations and using the robust CMAQ-PA results both quantifies and advances our understanding of the critical dynamical, physical, and chemical processes imparted by dense forest canopies, and emphasizes the need for their continued development in CTMs for both operational and community research applications. Overall, the inclusion of sub-canopy effects and their complex interactions challenge our fundamental understanding of the atmospheric state, in which the current suite of CTM and numerical weather prediction (NWP) models do not account for such interactions and rely on similarity theory and purely "big-leaf" approaches to describe the effects of dense forest canopies on such processes. As noted in Makar et al. (2017), impacts of forest shading and turbulence have similar or greater influence on near-surface ozone levels compared to climate change and current emissions policy scenarios. Thus, our work here further supports and demonstrates the importance of inclusion of such processes (even as relatively simple parameterizations) for the future of CTM, NWP, climate, and host of related Earth system models used to study the coupled atmosphere-biosphere interactions important for a myriad of applications.

Code availability:

https://doi.org/10.5194/egusphere-2025-485
Preprint. Discussion started: 16 May 2025

1. Canopy codes for CMAQv5.3.1: https://zenodo.org/records/14502375 (Campbell et al., 2024)
2. CMAQv5.3.1 (USEPA, 2024a)
3. Python 2.7 is used to treat the model output and can be downloaded on anaconda python website: https://www.anaconda.com/distribution/ (Anaconda, 2020)
4. R project for statistical computing can be downloaded at https://www.r-project.org (The R Foundation, 2021)
5. The process analysis tools and source codes including PseudoNetCDF, pyPA, and PERMM, can be downloaded on GitHub: https://github.com/barronh/pseudonetcdf, https://github.com/barronh/pypa, and https://github.com/barronh/permm (Henderson et al., 2009; Henderson et al., 2011)

Data availability:

1. The 2019 NEI emission model platform (EMP) and SMOKE model system can be downloaded on the EPA ftp website (USEPA, 2024b): https://www.epa.gov/air-emissions-modeling/2019-emissions-modeling-platform
2. The required additional vegetative canopy fields (e.g., FCH, LAI, CLU, POPU, FRT, and C1R-C4R; Figure 1) in their native and model-ready CMAQ domain and grid (processed by NACC; Campbell et al., 2022;2023) used here may be found at Zenodo: https://zenodo.org/records/14502375 (Campbell et al., 2024)
3. The meteorological ICs/BCs (based on regionally processed NOAA GFSv16) and representative fields used to drive the offline CMAQ model can be reproduced using the NACC software (Campbell et al., 2022); https://github.com/noaa-oar-arl/NACC or using web-based Cloud platform (Campbell, 2023); https://nacc.arl.noaa.gov/nacc/ . The NACC software can also be used to regrid and reprocess the vegetative canopy fields (#2 above) from native to desired CMAQ grid and domain configurations

Author contribution

https://doi.org/10.5194/egusphere-2025-485
Preprint. Discussion started: 16 May 2025

CTW and PCC are lead researchers in this study responsible for research design, experiments, analyzing, results and writing the manuscript. PM, BHB, BB, YT, and DT helped guide the research design and assessed model results. PM, SM, II, ZM, and RS prepare the canopy model input, canopy effect code and generate the model results, evaluations, and helped edit the manuscript.

Competing interests

The Authors declare that they have no conflict of interest.

Acknowledgments

We want to thank the National Oceanic and Atmospheric administration (NOAA) for supporting this study. This work is also supported by the Korea Environment Industry & Technology Institute (KEITI) through Climate Change R&D Project for New Climate Regime and the National Institute of Environmental Research (NIER) funded by Korea Ministry of Environment (MOE).

Financial Support

This study was funded by multiple sources: 1) NOAA grants NA24NESX432C0001 and NA19NES4320002 (Cooperative Institute for Satellite Earth System Studies -CISESS) at the University of Maryland/ESSIC, 2) NOAA/In-Canopy Processes Research based on NOAA Sponsor Number:NA22OAR4590516, and 3) Korea Environment Industry & Technology Institute (KEITI) through Climate Change R&D Project for New Climate Regime funded by Korea Ministry of Environment (MOE) (RS-2023-00232066). 4) The National Institute of Environmental Research (NIER), funded by the ministry of Environment (MOE) of the Republic of Korea (NIER-2024-01-02-033)

References

1. Alexander, B., Park, R. J., Jacob, D. J., and Gong, S.: Transition metal-catalyzed oxidation of atmospheric sulfur: Global implications for the sulfur budget, Journal of Geophysical Research: Atmospheres, 114, https://doi.org/10.1029/2008JD010486, 2009.

2. Anaconda python: https://www.anaconda.com/products/individual, last access: May, 1st, 2020.

3. Appel, K. W., Bash, J. O., Fahey, K. M., Foley, K. M., Gilliam, R. C., Hogrefe, C., Hutzell, W. T., Kang, D., Mathur, R., Murphy, B. N., Napelenok, S. L., Nolte, C. G., Pleim, J. E., Pouliot, G. A., Pye, H. O. T., Ran, L., Roselle, S. J., Sarwar, G., Schwede, D. B., Sidi, F. I., Spero, T. L.,

https://doi.org/10.5194/egusphere-2025-485
Preprint. Discussion started: 16 May 2025

and Wong, D. C.: The Community Multiscale Air Quality (CMAQ) model versions 5.3 and 5.3.1: system updates and evaluation, Geosci. Model Dev., 14, 2867-2897, 10.5194/gmd-14-2867-2021, 2021.

4. Ashworth, K., Chung, S. H., Griffin, R. J., Chen, J., Forkel, R., Bryan, A. M., and Steiner, A. L.: FORest Canopy Atmosphere Transfer (FORCAsT) 1.0: a 1-D model of biosphere–atmosphere chemical exchange, Geosci. Model Dev., 8, 3765-3784, 10.5194/gmd-8-3765-2015, 2015.

5. Baldocchi, D. D. and Harley, P. C.: Scaling carbon dioxide and water vapour exchange from leaf to canopy in a deciduous forest. II. Model testing and application, Plant, Cell & Environment, 18, 1157-1173, https://doi.org/10.1111/j.1365-3040.1995.tb00626.x, 1995.

6. Bash, J. O., Cooter, E. J., Dennis, R. L., Walker, J. T., and Pleim, J. E.: Evaluation of a regional air-quality model with bidirectional NH₃ exchange coupled to an agroecosystem model, Biogeosciences, 10, 1635-1645, 10.5194/bg-10-1635-2013, 2013.

7. Bonan, G. B., Williams, M., Fisher, R. A., and Oleson, K. W.: Modeling stomatal conductance in the earth system: linking leaf water-use efficiency and water transport along the soil–plant–atmosphere continuum, Geosci. Model Dev., 7, 2193-2222, 10.5194/gmd-7-2193-2014, 2014.

8. Bonan, G. B., Patton, E. G., Finnigan, J. J., Baldocchi, D. D., and Harman, I. N.: Moving beyond the incorrect but useful paradigm: reevaluating big-leaf and multilayer plant canopies to model biosphere-atmosphere fluxes – a review, Agricultural and Forest Meteorology, 306, 108435, https://doi.org/10.1016/j.agrformet.2021.108435, 2021.

9. Bonan, G. B., Patton, E. G., Harman, I. N., Oleson, K. W., Finnigan, J. J., Lu, Y., and Burakowski, E. A.: Modeling canopy-induced turbulence in the Earth system: a unified parameterization of turbulent exchange within plant canopies and the roughness sublayer (CLM-ml v0), Geosci. Model Dev., 11, 1467-1496, 10.5194/gmd-11-1467-2018, 2018.

10. Boy, M., Sogachev, A., Lauros, J., Zhou, L., Guenther, A., and Smolander, S.: SOSA – a new model to simulate the concentrations of organic vapours and sulphuric acid inside the ABL – Part 1: Model description and initial evaluation, Atmos. Chem. Phys., 11, 43-51, 10.5194/acp-11-43-2011, 2011.

11. Braghiere, R. K., Quaife, T., Black, E., He, L., and Chen, J. M.: Underestimation of Global Photosynthesis in Earth System Models Due to Representation of Vegetation Structure, Glob. Biogeochem. Cycle, 33, 1358-1369, https://doi.org/10.1029/2018GB006135, 2019.

12. Briggs, G. A.: A Plume Rise Model Compared with Observations, Journal of the Air Pollution Control Association, 15, 433-438, 10.1080/00022470.1965.10468404, 1965.

13. Bryan, A. M., Bertman, S. B., Carroll, M. A., Dusanter, S., Edwards, G. D., Forkel, R., Griffith, S., Guenther, A. B., Hansen, R. F., Helmig, D., Jobson, B. T., Keutsch, F. N., Lefer, B. L., Pressley, S. N., Shepson, P. B., Stevens, P. S., and Steiner, A. L.: In-canopy gas-phase

https://doi.org/10.5194/egusphere-2025-485
Preprint. Discussion started: 16 May 2025

907 chemistry during CABINEX 2009: sensitivity of a 1-D canopy model to vertical mixing and
908 isoprene chemistry, Atmos. Chem. Phys., 12, 8829-8849, 10.5194/acp-12-8829-2012, 2012.

909 14. Byun, D. and Schere, K. L.: Review of the Governing Equations, Computational
910 Algorithms, and Other Components of the Models-3 Community Multiscale Air Quality (CMAQ)
911 Modeling System, Applied Mechanics Reviews, 59, 51-77, 10.1115/1.2128636, 2006.

912 15. Science algorithms of the EPA Models-3 Community Multi-scale Air Quality (CMAQ)
913 modeling system:
914 https://cfpub.epa.gov/si/si_public_record_report.cfm?dirEntryId=63400&Lab=NERL last access:
915 January, 29, 2025.

916 16. GMU-SESS-AQ/CMAQ: GMU Canopy Tag for CMAQv5.3.1:
917 https://zenodo.org/records/14502375, last access: January 30, 2025.

918 17. The NOAA-EPA Atmosphere-Chemistry Coupler (NACC):
919 https://doi.org/10.5281/zenodo.10277248, last access: January 29, 2025.

920 18. Campbell, P. C., Tang, Y., Lee, P., Baker, B., Tong, D., Saylor, R., Stein, A., Huang, J.,
921 Huang, H. C., Strobach, E., McQueen, J., Pan, L., Stajner, I., Sims, J., Tirado-Delgado, J., Jung,
922 Y., Yang, F., Spero, T. L., and Gilliam, R. C.: Development and evaluation of an advanced
923 National Air Quality Forecasting Capability using the NOAA Global Forecast System version 16,
924 Geosci. Model Dev., 15, 3281-3313, 10.5194/gmd-15-3281-2022, 2022.

925 19. Chang, K.-Y., Paw U, K. T., and Chen, S.-H.: Canopy profile sensitivity on surface layer
926 simulations evaluated by a multiple canopy layer higher order closure land surface model,
927 Agricultural and Forest Meteorology, 252, 192-207,
928 https://doi.org/10.1016/j.agrformet.2018.01.027, 2018.

929 20. Chen, F. and Dudhia, J.: Coupling an Advanced Land Surface–Hydrology Model with the
930 Penn State–NCAR MM5 Modeling System. Part I: Model Implementation and Sensitivity,
931 Monthly Weather Review, 129, 569-585, https://doi.org/10.1175/1520-
932 0493(2001)129<0569:CAALSH>2.0.CO;2, 2001.

933 21. Chen, J.-H. and Lin, S.-J.: The remarkable predictability of inter-annual variability of
934 Atlantic hurricanes during the past decade, Geophysical Research Letters, 38,
935 https://doi.org/10.1029/2011GL047629, 2011.

936 22. Chen, J.-H. and Lin, S.-J.: Seasonal Predictions of Tropical Cyclones Using a 25-km-
937 Resolution General Circulation Model, Journal of Climate, 26, 380-398,
938 https://doi.org/10.1175/JCLI-D-12-00061.1, 2013.

939 23. Clifton, O. E., Patton, E. G., Wang, S., Barth, M., Orlando, J., and Schwantes, R. H.: Large
940 Eddy Simulation for Investigating Coupled Forest Canopy and Turbulence Influences on
941 Atmospheric Chemistry, Journal of Advances in Modeling Earth Systems, 14, e2022MS003078,
942 https://doi.org/10.1029/2022MS003078, 2022.

https://doi.org/10.5194/egusphere-2025-485
Preprint. Discussion started: 16 May 2025

24. Clough, S. A., Shephard, M. W., Mlawer, E. J., Delamere, J. S., Iacono, M. J., Cady-Pereira, K., Boukabara, S., and Brown, P. D.: Atmospheric radiative transfer modeling: a summary of the AER codes, Journal of Quantitative Spectroscopy and Radiative Transfer, 91, 233-244, https://doi.org/10.1016/j.jqsrt.2004.05.058, 2005.

25. Ek, M. B., Mitchell, K. E., Lin, Y., Rogers, E., Grunmann, P., Koren, V., Gayno, G., and Tarpley, J. D.: Implementation of Noah land surface model advances in the National Centers for Environmental Prediction operational mesoscale Eta model, Journal of Geophysical Research: Atmospheres, 108, https://doi.org/10.1029/2002JD003296, 2003.

26. Emery, C., Liu, Z., Russell, A. G., Odman, M. T., Yarwood, G., and Kumar, N.: Recommendations on statistics and benchmarks to assess photochemical model performance, Journal of the Air & Waste Management Association, 67, 582-598, 10.1080/10962247.2016.1265027, 2017.

27. Fuentes, J. D., Gerken, T., Chamecki, M., Stoy, P., Freire, L., and Ruiz-Plancarte, J.: Turbulent transport and reactions of plant-emitted hydrocarbons in an Amazonian rain forest, Atmospheric Environment, 279, 119094, https://doi.org/10.1016/j.atmosenv.2022.119094, 2022.

28. Gantt, B., Kelly, J. T., and Bash, J. O.: Updating sea spray aerosol emissions in the Community Multiscale Air Quality (CMAQ) model version 5.0.2, Geosci. Model Dev., 8, 3733-3746, 10.5194/gmd-8-3733-2015, 2015.

29. Gordon, M., Vlasenko, A., Staebler, R. M., Stroud, C., Makar, P. A., Liggio, J., Li, S. M., and Brown, S.: Uptake and emission of VOCs near ground level below a mixed forest at Borden, Ontario, Atmos. Chem. Phys., 14, 9087-9097, 10.5194/acp-14-9087-2014, 2014.

30. A description of the fifth-generation Penn State/NCAR Mesoscale Model (MM5), last

31. Guenther, A. B., Jiang, X., Heald, C. L., Sakulyanontvittaya, T., Duhl, T., Emmons, L. K., and Wang, X.: The Model of Emissions of Gases and Aerosols from Nature version 2.1 (MEGAN2.1): an extended and updated framework for modeling biogenic emissions, Geosci. Model Dev., 5, 1471-1492, 10.5194/gmd-5-1471-2012, 2012.

32. Han, J. and Bretherton, C. S.: TKE-Based Moist Eddy-Diffusivity Mass-Flux (EDMF) Parameterization for Vertical Turbulent Mixing, Weather and Forecasting, 34, 869-886, https://doi.org/10.1175/WAF-D-18-0146.1, 2019.

33. Han, J. and Pan, H.-L.: Revision of Convection and Vertical Diffusion Schemes in the NCEP Global Forecast System, Weather and Forecasting, 26, 520-533, https://doi.org/10.1175/WAF-D-10-05038.1, 2011.

34. Han, J., Wang, W., Kwon, Y. C., Hong, S.-Y., Tallapragada, V., and Yang, F.: Updates in the NCEP GFS Cumulus Convection Schemes with Scale and Aerosol Awareness, Weather and Forecasting, 32, 2005-2017, https://doi.org/10.1175/WAF-D-17-0046.1, 2017.

https://doi.org/10.5194/egusphere-2025-485
Preprint. Discussion started: 16 May 2025

978 35. Harman, I. N. and Finnigan, J. J.: A simple unified theory for flow in the canopy and
979 roughness sublayer, Boundary-Layer Meteorology, 123, 339-363, 10.1007/s10546-006-9145-6,
980 2007.

981 36. Harman, I. N. and Finnigan, J. J.: Scalar Concentration Profiles in the Canopy and
982 Roughness Sublayer, Boundary-Layer Meteorology, 129, 323-351, 10.1007/s10546-008-9328-4,
983 2008.

984 37. The python environment for reaction mechanism/mathematics (permm):
985 https://github.com/barronh/permm, last access: Nov16, 2024.

986 38. Henderson, B., Kimura, Y., McDonald-Buller, E., Allen, D. T., and Vizuete, W.:
987 Comparison of Lagrangian Process Analysis tools for Eulerian air quality models, Atmospheric
988 Environment, 45, 5200-5211, 10.1016/j.atmosenv.2011.06.005, 2011.

989 39. Henderson, B. H., Jeffries, H. E., Kim, B.-U., and Vizuete, W. G.: The Influence of Model
990 Resolution on Ozone in Industrial Volatile Organic Compound Plumes, Journal of the Air & Waste
991 Management Association, 60, 1105-1117, 10.3155/1047-3289.60.9.1105, 2010.

992 40. Hicks, B. B. and Baldocchi, D. D.: Measurement of Fluxes Over Land: Capabilities,
993 Origins, and Remaining Challenges, Boundary-Layer Meteorology, 177, 365-394,
994 10.1007/s10546-020-00531-y, 2020.

995 41. Hicks, B. B., Saylor, R. D., and Baker, B. D.: Dry deposition of particles to canopies—A
996 look back and the road forward, Journal of Geophysical Research: Atmospheres, 121, 14,691-
997 614,707, https://doi.org/10.1002/2015JD024742, 2016.

998 42. Iacono, M. J., Delamere, J. S., Mlawer, E. J., Shephard, M. W., Clough, S. A., and Collins,
999 W. D.: Radiative forcing by long-lived greenhouse gases: Calculations with the AER radiative
1000 transfer models, Journal of Geophysical Research: Atmospheres, 113,
1001 https://doi.org/10.1029/2008JD009944, 2008.

1002 43. Ivanova, I., Campbell, P.C., Makar, P., Hung., W.-T., Baker, B., Tang, Y., Moon, Z.,
1003 Saylor, R. D., Yang, F., Huang, J., Stajner, I., Montuoro, R.: Explicit Effects of Forest Canopy
1004 Shading and Turbulence on Boundary Layer Ozone in UFS-SRW Air Quality Model, 2024 AGU
1005 Conference, Washington, D.C.2024.

1006 44. Jeffries, H. E. and Tonnesen, S.: A comparison of two photochemical reaction mechanisms
1007 using mass balance and process analysis, Atmospheric Environment, 28, 2991-3003,
1008 https://doi.org/10.1016/1352-2310(94)90345-X, 1994.

1009 45. Jiménez, P. A., Dudhia, J., González-Rouco, J. F., Navarro, J., Montávez, J. P., and García-
1010 Bustamante, E.: A Revised Scheme for the WRF Surface Layer Formulation, Monthly Weather
1011 Review, 140, 898-918, https://doi.org/10.1175/MWR-D-11-00056.1, 2012.

1012 46. Kelly, J. T., Bhave, P. V., Nolte, C. G., Shankar, U., and Foley, K. M.: Simulating emission
1013 and chemical evolution of coarse sea-salt particles in the Community Multiscale Air Quality
1014 (CMAQ) model, Geosci. Model Dev., 3, 257-273, 10.5194/gmd-3-257-2010, 2010.

https://doi.org/10.5194/egusphere-2025-485
Preprint. Discussion started: 16 May 2025

47. Krueger, S. K., Fu, Q., Liou, K. N., and Chin, H.-N. S.: Improvements of an Ice-Phase Microphysics Parameterization for Use in Numerical Simulations of Tropical Convection, Journal of Applied Meteorology and Climatology, 34, 281-287, https://doi.org/10.1175/1520-0450-34.1.281, 1995.

48. Lin, Y.-L., Farley, R. D., and Orville, H. D.: Bulk Parameterization of the Snow Field in a Cloud Model, Journal of Applied Meteorology and Climatology, 22, 1065-1092, https://doi.org/10.1175/1520-0450(1983)022<1065:BPOTSF>2.0.CO;2, 1983.

49. Lord, S. J., Willoughby, H. E., and Piotrowicz, J. M.: Role of a Parameterized Ice-Phase Microphysics in an Axisymmetric, Nonhydrostatic Tropical Cyclone Model, Journal of Atmospheric Sciences, 41, 2836-2848, https://doi.org/10.1175/1520-0469(1984)041<2836:ROAPIP>2.0.CO;2, 1984.

50. Makar, P. A., Fuentes, J. D., Wang, D., Staebler, R. M., and Wiebe, H. A.: Chemical processing of biogenic hydrocarbons within and above a temperate deciduous forest, Journal of Geophysical Research: Atmospheres, 104, 3581-3603, https://doi.org/10.1029/1998JD100065, 1999.

51. Makar, P. A., Staebler, R. M., Akingunola, A., Zhang, J., McLinden, C., Kharol, S. K., Pabla, B., Cheung, P., and Zheng, Q.: The effects of forest canopy shading and turbulence on boundary layer ozone, Nature Communications, 8, 15243, 10.1038/ncomms15243, 2017.

52. Martin, L. R. and Good, T. W.: Catalyzed oxidation of sulfur dioxide in solution: The iron-manganese synergism, Atmospheric Environment. Part A. General Topics, 25, 2395-2399, https://doi.org/10.1016/0960-1686(91)90113-L, 1991.

53. Meyers, T. P., Finkelstein, P., Clarke, J., Ellestad, T. G., and Sims, P. F.: A multilayer model for inferring dry deposition using standard meteorological measurements, Journal of Geophysical Research: Atmospheres, 103, 22645-22661, https://doi.org/10.1029/98JD01564, 1998.

54. Mlawer, E. J., Taubman, S. J., Brown, P. D., Iacono, M. J., and Clough, S. A.: Radiative transfer for inhomogeneous atmospheres: RRTM, a validated correlated-k model for the longwave, Journal of Geophysical Research: Atmospheres, 102, 16663-16682, https://doi.org/10.1029/97JD00237, 1997.

55. Monin, A. and Obukhov, A. M.: BASIC LAWS OF TURBULENT MIXING IN THE GROUND LAYER OF ATMOSPHERE, Tr. Akad. Nauk SSSR Geophiz. Inst., 24(151), 163-187, 1954.

56. Monsi, M.: Uber den Lichtfaktor in den Pflanzengesellschaften und seine Bedeutung fur die Stoffproduktion, Japanese Journal of Botany, 14, 22-52, 1953.

57. Moon, Z., Fuentes, J. D., and Staebler, R. M.: Impacts of spectrally resolved irradiance on photolysis frequency calculations within a forest canopy, Agricultural and Forest Meteorology, 291, 108012, https://doi.org/10.1016/j.agrformet.2020.108012, 2020.

https://doi.org/10.5194/egusphere-2025-485
Preprint. Discussion started: 16 May 2025

58. Nilson, T.: A theoretical analysis of the frequency of gaps in plant stands, in: Agricultural Meteorology, P25-38, https://doi.org/10.1016/0002-1571(71)90092-6, 1971.

59. Norman, J. M.: Modeling the complete crop canopy, Modification of the Aerial Environment of Plants, American Society of Agricultural Engineers, St. Joseph, Michigan1979.

60. Ogée, J., Brunet, Y., Loustau, D., Berbigier, P., and Delzon, S.: MuSICA, a CO2, water and energy multilayer, multileaf pine forest model: evaluation from hourly to yearly time scales and sensitivity analysis, Global Change Biology, 9, 697-717, https://doi.org/10.1046/j.1365-2486.2003.00628.x, 2003.

61. Pleim, J. and Ran, L.: Surface Flux Modeling for Air Quality Applications, Atmosphere, 2, 271-302, 10.3390/atmos2030271, 2011.

62. Pleim, J. E., Bash, J. O., Walker, J. T., and Cooter, E. J.: Development and evaluation of an ammonia bidirectional flux parameterization for air quality models, Journal of Geophysical Research: Atmospheres, 118, 3794-3806, https://doi.org/10.1002/jgrd.50262, 2013.

63. Pleim, J. E., Ran, L., Appel, W., Shephard, M. W., and Cady-Pereira, K.: New Bidirectional Ammonia Flux Model in an Air Quality Model Coupled With an Agricultural Model, Journal of Advances in Modeling Earth Systems, 11, 2934-2957, https://doi.org/10.1029/2019MS001728, 2019.

64. Pleim, J. E., Ran, L., Saylor, R. D., Willison, J., and Binkowski, F. S.: A New Aerosol Dry Deposition Model for Air Quality and Climate Modeling, Journal of Advances in Modeling Earth Systems, 14, e2022MS003050, https://doi.org/10.1029/2022MS003050, 2022.

65. Raupach, M. R.: A practical Lagrangian method for relating scalar concentrations to source distributions in vegetation canopies, Quarterly Journal of the Royal Meteorological Society, 115, 609-632, https://doi.org/10.1002/qj.49711548710, 1989.

66. Sarwar, G., Fahey, K., Napelenok, S., Roselle, S., and Mathur, R.: Examining the impact of CMAQ model updates on aerosol sulfate predictions, The 10th Annual CMAS Models-3 User's Conference, Chapel Hill, NC, US2011.

67. Saylor, R. D.: The Atmospheric Chemistry and Canopy Exchange Simulation System (ACCESS): model description and application to a temperate deciduous forest canopy, Atmos. Chem. Phys., 13, 693-715, 10.5194/acp-13-693-2013, 2013.

68. Saylor, R. D., Baker, B. D., Lee, P., Tong, D. Q., Pan, L., and Hicks, B. B.: The particle dry deposition component of total deposition from air quality models: right, wrong or uncertain?, Tellus B: Chemical and Physical Meteorology, 71, 2019.

69. Schwede, D. B., Pouliot, G. A., and Pierce, T.: CHANGES TO THE BIOGENIC EMISSIONS INVENTORY SYSTEM VERSION 3 (BEIS 3),

70. Stroud, C., Makar, P., Karl, T., Guenther, A., Geron, C., Turnipseed, A., Nemitz, E., Baker, B., Potosnak, M., and Fuentes, J. D.: Role of canopy-scale photochemistry in modifying biogenic-

https://doi.org/10.5194/egusphere-2025-485
Preprint. Discussion started: 16 May 2025

1088 atmosphere exchange of reactive terpene species: Results from the CELTIC field study, Journal of
1089 Geophysical Research: Atmospheres, 110, https://doi.org/10.1029/2005JD005775, 2005.

1090 71. Tewari, M., Chen, F., Wang, W., Dudhia, J., LeMone, M. A., Mitchell, K., Ek, M., Gayno,
1091 G., Wegiel, J., and Cuenca, R. H: Implementation and verification of the unified NOAH land
1092 surface model in the WRF model, 20th Conference on Weather Analysis and Forecasting/16th
1093 Conference on Numerical Weather Prediction, Seattle, WA2004.

1094 72. The R Project for Statistical Computing: https://www.r-project.org, last access: Jan, 25th,
1095 2022, 2022.

1096 73. CMAQ User's Guide, last access: January 29, 2025.

1097 74. CMAQ: The Community Multiscale Air Quality Modeling System:
1098 https://www.epa.gov/cmaq, last access: January 30, 2025.

1099 75. 2019 Emissions Modeling Platform (EMP): https://www.epa.gov/air-emissions-
1100 modeling/2019-emissions-modeling-platform, last access: Nov 03, 2022.

1101 76. Vermeuel, M. P., Millet, D. B., Farmer, D. K., Pothier, M. A., Link, M. F., Riches, M.,
1102 Williams, S., and Garofalo, L. A.: Closing the Reactive Carbon Flux Budget: Observations From
1103 Dual Mass Spectrometers Over a Coniferous Forest, Journal of Geophysical Research:
1104 Atmospheres, 128, e2023JD038753, https://doi.org/10.1029/2023JD038753, 2023.

1105 77. The Implementation of BEIS3 within the SMOKE modeling framework:
1106 https://www.epa.gov/sites/default/files/2015-10/documents/vukovich.pdf, last access: January 31,
1107 2025.

1108 78. Wolfe, G. M. and Thornton, J. A.: The Chemistry of Atmosphere-Forest Exchange (CAFE)
1109 Model – Part 1: Model description and characterization, Atmos. Chem. Phys., 11, 77-101,
1110 10.5194/acp-11-77-2011, 2011.

1111 79. Xu, L., Pyles, R. D., Paw U, K. T., Snyder, R., Monier, E., Falk, M., and Chen, S.-H.:
1112 Impact of canopy representations on regional modeling of evapotranspiration using the WRF-
1113 ACASA coupled model, Agricultural and Forest Meteorology, 247, 79-92,
1114 https://doi.org/10.1016/j.agrformet.2017.07.003, 2017.

1115 80. CB6 Version 6 of the Carbon Bond Mechanism:
1116 https://www.eoas.ubc.ca/courses/atsc507/ADM/cmaq/cb6.pdf, last access: January 31, 2025.
1117